MODELING OF REINFORCED CONCRETE MEMBRANE BEHAVIOR CONSIDERING SHEAR STRESS TRANSFER ACROSS CRACKS

by

Emir Hazar Bekaroğlu

B.S., Civil Engineering, Yıldız Technical University, 2014

Submitted to the Institute for Graduate Studies in
Science and Engineering in partial fulfillment of
the requirements for the degree of
Master of Science

Graduate Program in Civil Engineering

Boğaziçi University

2019

MODELING OF REINFORCED CONCRETE MEMBRANE BEHAVIOR CONSIDERING SHEAR STRESS TRANSFER ACROSS CRACKS

APPROVED BY:

Assoc. Prof. Kutay Orakçal (Thesis Supervisor)	.....
Assoc. Prof. Özer Çinicioğlu	.....
Assist. Prof. Zeynep Tuna Değer	.....

DATE OF APPROVAL: 30.05.2019

To my family

ACKNOWLEDGEMENTS

First and foremost, I would like to express my sincere gratitude to Assoc. Prof. Kutay Orakçal for his continuous support, patience and guidance, all will be remembered long after this research is completed. Leading by example and having supported me not just as a student but also as a professional, the lessons he thought me throughout my time in Boğaziçi University will always be immensely appreciated.

Having his doors open with a positive and practical approach at all times, I would also like to thank M. Fethi Güllü, without his support on the modelling side none of this would be possible.

Also, I would like to thank the esteemed members of my thesis examination committee, Assoc. Prof. Özer Çinicioğlu and Assist. Prof. Zeynep Tuna Değer, for taking the time from their busy schedules and for sharing their valuable thoughts.

I would also like to thank my old friend Yağız Erçin for his companionship since my undergraduate years and for his support during the preparation of this thesis. Remembering all my other civil engineer friends, I hereby thank them for creating so many memories to cherish. Additionally, special thanks to my friend, Semih Gönen, who widened my perspective and supported me during my graduate years and my colleagues who supported me to complete this thesis despite everything.

For spreading their passion of civil engineering and for their encouragement, I would also like to send my gratitude to Prof. Bilge Doran and Assoc. Prof. Murat Altekin. Finally, I want to thank my dear parents and sister for being there in good and bad times. My father, Özhan Bekaroğlu, who passed on his passion for engineering, my mother, M. Vuslat Bekaroğlu, who thought me how to be patient and my sister, M. Gökçe Bekaroğlu, for being the best companion one could ever ask for. I will remain forever in your debt.

ABSTRACT

MODELING OF REINFORCED CONCRETE MEMBRANE BEHAVIOR CONSIDERING SHEAR STRESS TRANSFER ACROSS CRACKS

In this study, a previously-developed reinforced concrete panel (membrane) model formulation is improved by incorporating simple yet effective constitutive relationships that simulate shear transfer mechanisms across cracks. First, a friction-based shear aggregate interlock mechanism with cyclic degradation parameters is incorporated. Second improvement is the implementation of an origin-oriented dowel action model on reinforcing bars with cyclic degradation parameters. These mechanical enhancements are aimed to achieve better simulation of test results with consideration of physical phenomenon's (e.g. friction along cracks, dowel action, degradation) that are neglected (in full or partially) in the formulations of other panel models available in the literature. Improved model is further validated against test results from two different experimental programs. Sensitivity of the improved model to the coefficient of friction is evaluated through computational analyses carried out on five different panel specimens that are identified as sensitive to the applied shear transfer mechanisms due to their design or loading characteristics (e.g. asymmetric or inclined reinforcement, complicated loading conditions). Thereafter, using optimal friction coefficients obtained by the parametric sensitivity analysis results, global and local response predictions of the model for ten different panel specimens (including specimens used for sensitivity analyses) are compared with test results from two different experimental programs for validation of the improved model. Finally, it was observed that the improved panel model provides good correlation with test results as majority of the results are indeed satisfactory.

ÖZET

BETONARME MEMBRAN ELEMANLARIN ÇATLAKLAR ARASI KAYMA GERİLME AKTARIMININ DİKKATE ALINARAK MODELLENMESİ

Bu çalışmada, betonarme davranışını temsil etmek için daha önceden geliştirilmiş olan bir panel (membran) modeli, çatlak boyunca oluşan kaymaya karşı çalışan direnç mekanizmaları ile iyileştirilmiş ve yeni modelin deneysel doğrulama çalışmaları yürütülmüştür. İlk olarak modele agrega kenetlenmesi yoluyla çatlak yüzeyinde açığa çıkan sürtünme temelli kayma gerilme aktarım mekanizması ve ilgili döngüsel degradasyon parametreleri eklenmiştir. İkinci geliştirme ise merkez-odaklı dübel hareket modeli ve ilgili döngüsel degradasyon parametreleri modele eklenmiştir. Bu mekanik geliştirmelerin amacı, literatürdeki diğer membran modellerinin formülasyonlarında tamamen veya kısmen ihmal edilen bazı olası fiziksel olayların (örneğin, çatlaklar arası sürtünme, dübel hareketleri ve döngüsel davranış sebebiyle beklenen davranış degradasyonu) da hesaba katılarak modellenmesi ve test sonuçlarına daha yakın sonuçlar elde edilmesidir. Geliştirilen model daha sonra iki farklı deneysel program ile kıyaslanarak doğrulanmıştır. Geliştirilen bu modelin sürtünme katsayısına olan hassasiyeti sayısal analizler aracılığıyla, bu katsayıya tasarım veya yükleme koşulları sebebiyle (örneğin, asimetrik veya açılı donatıya sahip ve/veya karmaşık yükleme koşulları altında) hassas olduğu tespit edilen beş farklı membran eleman üzerinde değerlendirilmiştir. Daha sonra, hassasiyet analizleri sonucu elde edilen optimum sürtünme katsayılarını geliştirilen modelde kullanarak elde edilen küresel ve bölgesel model sonuçları aynı on farklı panel/membranın deney sonuçlarıyla kıyaslanmış ve geliştirilen modelin sonuçları böylece doğrulanmıştır. Sonuç olarak, geliştirilen panel modelin sonuçlarının çoğunlukla tatmin edici olduğu ve deney sonuçlarıyla iyi bir korelasyon gösterdiği gözlemlenmiştir.

TABLE OF CONTENTS

LIST OF FIGURES

LIST OF TABLES

LIST OF SYMBOLS

A_S	Sectional area of reinforcement
$a_1 and a_2$	Experimentally obtained parameters
b	Strain hardening ratio
d_b	Reinforcing bar diameter
E_o	Modulus of elasticity
E_1	Yield modulus
E_c	Elastic shear modulus of concrete
E_s	Modulus of elasticity for steel
$E_c E1i$	Increment step number
$F_{D,deg}$	Dowel force with cyclic degradation
f_c	Concrete compressive strength
f_t	Concrete tensile strength
f'_c	Peak compressive stress
k_c	Foundation modulus of the surrounding concrete
K_D	Secant stiffness
l	Effective dowel length
R	Curvature parameter
R_0	Curvature parameter value assigned at start
s	Shear displacement or slip deformation
$\|s_{max}\|$	Max shear displacement or slip deformation
V_{dow}	Dowel force
$V_{dow,deg}$	Dowel force with degradation
w	Crack opening
α	Degradation parameter
α_2	Steel bar orientation in Mansour and Hsu panels
β	Compression softening parameter
γ_{dow}	Dowel strain
γ_{xy}	Shear Strain

Δ	Dowel deformation
Δ_crack	Slip deformation at crack interface
Δ_dow	Slip deformation - dowel
Δ	Load increment
$\Delta\delta$	Displacement increment
$(\Delta\delta)_n$	Initial displacement increment
$(\Delta\lambda)_i$	Load increment at step i
$(\Delta\delta)_i$	Displacement increment at step i
δ	Displacement
δ_i	Displacement at step i
ε	Strain
ε_t	Concrete tensile strain at peak tension stress
ε_{pl}	Plastic strain upon loading
ε_i	Principal strain in direction 1
ε_2	Principal strain in direction 2
ε_x	Principal strain in x-direction
ε_y	Principal strain in y-direction
$\varepsilon_{x'}$	Arbitrary strain transformed to x'-direction
$\varepsilon_{y'}$	Arbitrary strain transformed to y'-direction
θ	Principal strain direction for the uncracked concrete
θ_{crA}	Concrete crack direction A or Fixed Strut Angle A
θ_{crB}	Concrete crack direction B or Fixed Strut Angle B
λ	Load parameter
λ	Relative stiffness of the foundation
λ_i	Load at step i
ξ	Absolute strain difference between current asymptote and previous reversal point
ρ_l	Longitudinal reinforcement ratio
ρ_s	Reinforcement ratio in crack direction
ρ_{sx}	Steel reinforcement ratio in x-direction
ρ_{sy}	Steel reinforcement ratio in y-direction
ρ_t	Reinforcement ratio (total)

ρ_x	Reinforcement ration in x-direction
ρ_y	Reinforcement ratio in y-direction
σ	Stress
σ_c	Compressive stress on concrete
σ_{c1}	Principal concrete stress in direction 1
σ_{c2}	Principal concrete stress in direction 2
σ_{cx}	Concrete stress in x-direction
σ_y	Concrete stress in y-direction
$\sigma_{cx'}$	Concrete stress in x'-direction
$\sigma_{cy'}$	Concrete stress in y'-direction
σ_H	Stress applied in H direction
σ_s	Tensile stress on steel reinforcement
σ_{sx}	Softened concrete stress in x-direction
σ_{sy}	Softened concrete stress in y-direction
σ_V	Stress applied in V direction
σ_x	Total normal stress in x-direction
σ_y	Total normal stress in y-direction
$\sigma_{\perp c}$	Constant compressive stress
τ_{xy}	Total shear stress
τ_{cxy}	Total shear stress
$\tau_{x'y'}$	Resultant shear stress in adopted shear aggregate interlock model
$\gamma_{x'y'}$	Sliding shear strain in adopted shear aggregate interlock model
τ_{total}	Superimposed resultant stress
τ_{agr}	Stress due to friction-based shear aggregate interlock
τ_D	Stress due to dowel action on reinforcing bars
τ_{fr}	Shear stress (friction) in
$\tau_{crack,deg}$	Friction force with degradation

1. INTRODUCTION

1.1. General

As the analysis and design of structural members subjected to earthquake ground motion are carried out under consideration of performance-based design approaches, nonlinear modeling of behavioral characteristics of structural members subjected to cyclic loading a more remarkable topic among researchers. Existing computer software's for structural engineers are used for simulation of the time-dependent behavior of structural systems (e.g. bridges, buildings, dams etc.) subjected to earthquake ground motion. However, studies show that analytical models available in the literature are not capable of simulating nonlinear hysteretic responses of 2D elements (e.g., walls).

In many countries (including Turkey, which is located in a seismically active region), using reinforced concrete (RC) structural walls were not as common as RC frames, which may be attributed to unawareness of the engineers about the advantages of using structural walls or dual systems despite their significant contributions to seismic resistance of reinforced concrete structural systems. When structural systems are designed and detailed using performance-based design approaches, they are found to be capable of providing deformation capacities or ductility demands against moderate or severe earthquake ground motions while conserving the lateral stiffness and lateral load capacities. However, most of the existing structures in Turkey (e.g. ones built before the Izmit earthquake in 1999) were not built using sufficient number of RC structural walls (Bal *et al.*, 2008).

Although they were not used widely, structural walls used in construction of thethat were built for constructing these older buildings in the past have experienced shear failure instead of flexural failure when subjected to earthquake ground motionmotions since they were not designed in accordance with thetheir performance-based needs (e.g. ductility demands or deformation capacities).

With increasing awareness of advantages of using RC structural walls, recent studies have focused on the behavioral characteristics of RC structural walls. Well-detailed and designed slender walls are more susceptible to fail under flexure, meaning that response of these walls is governed by flexure. For analysis and design of these walls, a simple analytical model considering nonlinear flexural behavior is necessary. On the other hand, squat walls (or walls representing shear -controlled responses), which are considered to have aspect ratios (effective height divided by width) smaller than 1.5, more probably undergo shear failure, which results in sudden degradation in strength and stiffness of the walls. This non-ductile behavior of squat walls makes their global and local responses more susceptible to parameters associated with shear strength and stiffness.

Simple analysis methods available in literature (e.g., moment-curvature analysis) or more detailed ones (e.g., fiber-based analysis) can reasonably capture the lateral load vs. deformation response characteristics of slender walls; however, they are not capable of simulating the coupled effect of axial-flexural-shear responses. Recent experimental observations revealed that uncoupling of axial, shear and flexural responses leads to inadequacy in predicting the experimental results. Hence, an analytical model that can capture the coupling of effects of axial, shear and flexural responses is required.

Based on the identified weaknesses of the existing modeling approaches used for RC structural walls addressed in the previous paragraphs, need for analytical models that can provide accurate response predictions is obvious and more studies focusing on such shortcomings are inevitable. It is significant to emphasize that modeling of RC structural walls with reasonable accuracy is possible with introduction of a robust membrane model that can capture nonlinear behavior of RC membrane elements under generalized, in-plane, reversed-cyclic loading conditions. A novel constitutive model named Fixed-Strut-Angle Model (FSAM) was proposed by Ulugtekin in 2010 for the same purposes. Notwithstanding its promising results, the developed model still needs further improvements, especially in shear transfer mechanisms along cracks. Within the scope of this study, FSAM is further improved via incorporating cyclic constitutive relationships for shear aggregate interlock and dowel action mechanisms with their

cyclic degradation parameters for simulating the impacts of such behavioral features in predicting the response of reinforced concrete (RC) panel elements. The validity of the improved model is also shown by comparing the model predictions with test results obtained from literature.

1.2. Background

The pioneers of the membrane models available in literature are Modified Compression Field Theory (MCFT) proposed by Vecchio and Collins (1986), modified after the Diagonal Compression Field Theory (Mitchell and Collins 1974) to take into account the tensile stresses in concrete between cracks while also employing experimentally verified average stress strain relationships for the cracked concrete, and Rotating Angle Softened Truss Model (Pang and Hsu 1995), as a follow up to earlies studies by Mau and Hsu (1986), Mau and Hsu (1987) and Hsu (1988).

Both milestone models followed the rotating-angle approach, applicable in monotonic loading conditions, and were capable of modeling reinforced concrete panel (membrane) element behavior. One of the several inherent assumptions of these models was the perfect bond between materials (i.e. concrete and rebars) where (i) for concrete in tension and compression uniaxial constitutive formulations were applied along the principal strain directions, and (ii) for steel, constitutive relationships in similar nature (i.e. uniaxial) were implemented along the rebar axis. Vecchio and Collins (1986), also showed that cracked concrete subjected to high tensile strains in the direction normal to the compression was actually "softer and weaker" than concrete properties observed in a standard cylinder test and therefore cracked concrete was treated as a new material having unique stress-strain behavioral characteristics in membrane models. Based on these findings, various relationships were suggested that could help to transform average strains to average stress in virtue of the incorporated smeared (average) stress-strain approach. Both the perfect bond assumption and the smeared crack approach were used in most of the subsequent studies and models as they were reasonable and practical.

Although these models are pioneers of membrane modeling and they were practical, since they had monotonic stress-strain relationships for concrete and steel materials they were not applicable in modeling of membrane models subjected to cyclic loading. Furthermore, underlying assumption of whether principal stresses and strains were coinciding or not created complexities during the physical interpretation of membrane behaviors. In real behavior of reinforced concrete membrane elements, when a crack is formed, the direction of the crack remains same (more or less), revealing that using rotating angle modeling approach after formation of cracks leads to behavioral variations between practice and theory. Therefore, instead of using rotating angle modeling approaches, some researchers proposed a modeling approach that assumes a fixed-crack angle after formation of cracks (Pang and Hsu 1995, Hsu and Zhu 2002, Mansour and Hsu 2005). Common assumption in rotating angle models of coinciding principal stress directions and principal strain directions in concrete was changed to that of principal stress directions in concrete were fixed to crack directions in reinforced concrete membrane elements. Taking this assumption into consideration, some models in literature assumed an "angle lag" approach (e.g. Vecchio 2000, Stevens 1991) where principal stresses were not in the same directions with principal strains.

In addition to the monotonic constitutive panel models, other constitutive panel models with similar approaches (e.g. rotating and fixed-crack angle) but that can be applicable under cyclic loading conditions (e.g. Ohmori*et al.* 1989, Stevens accessed at October 1991, Vecchio 1999, Palermo and Vecchio 2003, Mansour and Hsu 2005, Gerin and Adebar 2009) have been proposed by other researchers. These models were based on one or more of three cyclic experimental studies carried out by Ohmori *et al.* (1989), Mansour and Hsu (2005) and Stevens (1987). Although researchers have made attempts on proposing a more developed analytical model, nearly none of these models were implemented in open-source computational structural analysis platforms (e.g. OpenSees, McKenna *et al.* 2000) and even if they are, studies on the ones available are not extensive enough for allowing public usage (e.g. by designers or other professionals).

Researchers who developed membrane models also interpreted the shear trans-

fer mechanisms along crack directions differently. In some models shear stress transfer across cracks would be transmitted only by frictional force, whereas in some other models shear resisting mechanism was accomplished by adding clamping force to frictional force. Slightly different than the former, Modified Compression Field Theory by Vecchio and Collins (1986) considered frictional resistance by incorporating an empirical equation along crack interface. However, most of the models available in literature did not incorporate an all-inclusive shear transfer mechanism (composed of shear aggregate interlock along crack surface and dowel action on reinforcing bars) across cracks. Since membrane models did not consider these mechanisms or physical phenomenon's, validity of these model against simulation of the interaction between axial, flexural and shear deformations are not proven.

Unless the surface is perfectly smooth between cracks, a shear aggregate interlock (when looking at it in microscopic level) phenomenon can be observed along the crack surface. In addition to the observed aggregate interlock mechanisms, resisting effects of steel reinforcements intersecting the crack surface results in dowel action on the reinforcing steel. Before dowel action was studied in literature, researchers have been investigating only the effects of the aggregate interlock mechanism. Dowel action was investigated by researchers; He and Kwan (2001), Vintzeleou and Tassios (1987 and 1990), Maekawa and Qureshi (1996). Dowel model proposed by He and Kwan (2001) differentiate from others as it was compatible with the common inherent assumption of other models, which was the smeared crack approach. Observations focusing on the phenomenon were made by researchers like Mattock and Hawkins (1972), Walraven (1981), Hsu *et al.*, (1987), Martin-Perez and Pantazopulou (1999), Theodossius *et al.*, (1987) and Palieraki and Vintzileou (2009) where outcomes of the studies made by the latter two showed that cyclic loading caused degradation in shear responses, meaning that a cyclic degradation parameter on shear transfer mechanisms applied across cracks may also need to be considered in future modeling attempts.

1.3. Research Significance

RC structural walls are used in design of structural systems due to their significant contribution to the seismic- resistance of the overall structure. Although modeling of relatively slender RC structural walls can be achieved by using the existing modeling approaches in literature due to their flexure dominant responses, modeling of medium-rise walls (aspect ratios between 1.5 and 2.0) having coupled effect of shear-flexural interaction in their responses and squat walls (aspect ratios less than 1.0) with nonlinear shear responses is still not well-simulated by the analytical models available in literature. To propose a simple and reasonably accurate membrane model which can be used in modeling approaches that consider the interaction (coupling) of axial, flexural and shear responses, and capable of capturing the hysteretic responses with incorporation of a reliable shear transfer mechanism along cracks is therefore found to be necessary for predicting the nonlinear shear behavior and/or shear flexural interaction responses of RC walls.

1.3.1. Objectives

Based on the shortcomings identified in literature and following the studies conducted by Ulugtekin (2010) and Orakcal *et al.*, (2012) for developing the "Fixed Strut Angle Model" (FSAM), the objective of this study is to improve the FSAM via modifying the previously implemented friction based elasto-plastic shear aggregate interlock model by adding a cyclic degradation parameter and by implementing an origin-oriented dowel action model that also considers cyclic degradation parameter. The improved model is validated against test results provided by Stevens (1987) and Mansour and Hsu (2005) on RC panel specimens. Additionally, sensitivity of the improved FSAM against model parameters (i.e. coefficient of friction defined in the elasto-plastic shear aggregate interlock model) that dominates the shear transfer across cracks.

1.3.2. Scope

Scope of this study includes the following:

- A brief review of constitutive panel models and shear transfer mechanisms available in the literature and outlining their general characteristics as well as their irregularities and weaknesses,
- Improving the originally proposed FSAM formulation by implementing constitutive models for simulating the shear transfer mechanisms along cracks,
- Sensitivity analysis for the improved model against variations in the model parameters (i.e. friction coefficient),
- Comparison of improved model results with the test results on RC panel specimens provided by Stevens (1987) and Mansour and Hsu (2005).

1.3.3. Thesis Outline

In the first chapter (Chapter 1), the available literature is briefly reviewed, and objectives and scope of the study are detailed following the brief introduction to the topic. Chapter 2 briefly summarizes the working principles of the FSAM and followed by explaining the hysteretic constitutive material models that are available in the model formulation for reinforcing steel and concrete together with the empirical formulations used for consideration of the behavioral features (i.e. tension stiffening, compression softening, biaxial damage behavior). Chapter 3 introduces the improvements made on the analytical model within the scope of this study. Results of sensitivity analyses carried out using the improved model shown in Chapter 4 and optimal friction coefficients for each of the test results are proposed in accordance with the comparison of model results against experimental results provided by Stevens (1987) and Mansour and Hsu (2005). Last chapter (Chapter 5) concludes the study by discussing the results of the analytical model with consideration of the suggested improvements and provides recommendations for future studies.

2. MODEL DESCRIPTION

Although having common assumptions with models available in literature (e.g. perfect bond between concrete and rebar, no dowel action on reinforcement) the Fixed Strut Angle Model (FSAM) proposed by Ulugtekin (2010) stands out from other models with its simplistic features and working mechanism. As an example, unlike other models considering the fixed-crack angle approach (e.g., Pang and Hsu 1995, Hsu and Zhu 2002, Mansour and Hsu 2005), the proposed Fixed Strut Angle Model does not require proportional loading as it does not assume that fixed crack directions coincide with the applied stress direction after formation of the first crack. Working mechanism of FSAM is explained in further detail in the following sub-sections of this chapter.

Another advantage of the FSAM is that its baseline formulation is flexible, meaning that various behavioral models can be implemented and modified (e.g. model for shear stress transfer across cracks). Considering the flexibility of the model, improvements were made on top of FSAM's baseline formulation, to consider actual physical phenomenon's relating to shear stress transfer mechanism across cracks. These improvements are also summarized in Chapter 3.

2.1. Working Principals of the Panel Model

Until the first crack is formed in the concrete (i.e. during the uncracked state) the model assumes a rotating-strut approach for representing the stress-strain behavior of the uncracked panel element. Similar approach can also be observed in some of the earlier modelling efforts summarized in Section 1.2. (e.g. Modified Compression Field Theory by Vecchio and Collins 1986 and the Rotating-Angle Softened Truss Model by Pang and Hsu 1995). Using a displacement-based formulation, for which a strain field is applied first $(\varepsilon_x, \varepsilon_y, \tau_{xy})$ the principal strain directions (θ_p) of the uncracked panel and corresponding principal strains $(\varepsilon_1, \varepsilon_2)$ can be obtained as illustrated in Figure 2.1a. Following the calculation of the principal strains, unsoftened principal stresses in concrete are obtained via the monotonic envelope of the constitutive material model

(see following sections for further details on material models). Such principal stress directions are assumed to coincide and rotate together with the principal strain directions during the uncracked stage. The stress-strain relationships used to obtain principal stresses in concrete are uniaxial, however, FSAM formulation includes softening parameters to incorporate compression softening or biaxial damage. Meaning, the obtained concrete stresses are trimmed via applicable compression softening parameters to obtain σ_{c1} and σ_{c2} (softened principal stresses).

After following the steps described above, uniaxial stress values $(\sigma_s x, \sigma_s y)$ for reinforcing steel bars are calculated using the normal strains applied in the oriented direction of reinforcing steel bars. To obtain reinforcing steel stress values, the monotonic envelope of the constitutive steel model is used in both orthogonal directions, along x and y axes, which should coincide with reinforcement directions either by geometrical arrangements of the panel or naturally. Superposition of the concrete and reinforcing steel stress values along x and y directions is conducted by the following transformation equations:

$$\sigma_x = \frac{\sigma_{c1} + \sigma_{c2}}{2} + \frac{\sigma_{c1} - \sigma_{c2}}{2} \cdot cos2\theta + \rho_{sx} \cdot \sigma_{sx} \tag{2.1}$$

$$\sigma_y = \frac{\sigma_{c1} + \sigma_{c2}}{2} - \frac{\sigma_{c1} - \sigma_{c2}}{2} \cdot cos2\theta + \rho_{sy} \cdot \sigma_{sy} \tag{2.2}$$

$$\tau_{xy} = \frac{\sigma_{c1} - \sigma_{c2}}{2} \cdot sin2\theta \tag{2.3}$$

Once the principal tensile strain in concrete is equal to or larger than the monotonic cracking strain of concrete (ε_t in Figure 2.2) a crack is formed (first crack) in perpendicular direction to the principal tensile strain. At the instance of the formation of the first crack direction ($\theta_c rA$), the "first fixed strut" direction of the membrane is also formed (Figure 2.1b). Although the principal strain directions corresponding to

applied strain field may rotate, the principal stress directions are fixed (along and perpendicular to the first fixed strut directions). This assumption implies zero aggregate interlock across the crack interface since the strut directions are always coinciding with principal stress directions in concrete. Uniaxial strains $(\varepsilon'_x, \varepsilon'_y)$ of concrete along the first crack direction are derived as follows, here $\theta_c rA$ represents the "first fixed strut" direction of the panel:

$$\varepsilon_{x'} = \frac{\varepsilon_x + \varepsilon_y}{2} + \frac{\varepsilon_x - \varepsilon_y}{2} \cdot cos2\theta_{crA} + \frac{\gamma_{xy}}{2} \cdot sin2\theta_{crA} \tag{2.4}$$

$$\varepsilon_{y'} = \frac{\varepsilon_x + \varepsilon_y}{2} - \frac{\varepsilon_x - \varepsilon_y}{2} \cdot cos2\theta_{crA} - \frac{\gamma_{xy}}{2} \cdot sin2\theta_{crA} \tag{2.5}$$

After obtaining the uniaxial strains in the fixed strut directions and considering that the principal stress directions are fixed along these directions as well as the employment of a uniaxial hysteretic stress-strain relationship for concrete, principal stress values are easily recorded in the directions parallel and perpendicular to the first fixed strut direction. Similar to the uncracked response calculations, compression softening, and biaxial damage parameters are considered to soften the concrete stresses based on the experimentally-observed behavioral features for concrete specimens tested under biaxial loading. Finally, uniaxial stresses for reinforcing steel bars are again calculated with the same approach used for uncracked concrete. Following the application of softening effects in concrete and calculation of steel stresses, stress values of the panel element in the $x - y$ coordinate system are derived as follows:

$$\sigma_x = \frac{\sigma_{cx'} + \sigma_{cy'}}{2} + \frac{\sigma_{cx'} - \sigma_{cy'}}{2} \cdot cos2\theta_{crA} + \rho_{sx} \cdot \sigma_{sx} \tag{2.6}$$

$$\sigma_y = \frac{\sigma_{cx'} + \sigma_{cy'}}{2} - \frac{\sigma_{cx'} - \sigma_{cy'}}{2} \cdot cos2\theta_{crA} + \rho_{sy} \cdot \sigma_{sy} \tag{2.7}$$

$$\tau_{xy} = \frac{\sigma_{cx'} - \sigma_{cy'}}{2} \cdot sin2\theta_{crA} \tag{2.8}$$

At the point where the tensile strain in the first fixed strut direction goes beyond the cracking strain of the concrete ($\varepsilon_{c0} + \varepsilon_t$in Figure 2.2), the second crack is formed in perpendicular direction to the original (first) crack, due to the zero aggregate interlock assumption (Figure 2.1c). With continuous loading in subsequent steps, the two "fixed struts" (first and second) work in tension or compression interchangeably, related to the direction of the principal strains resulting from the applied strain fields on the panel element. Uniaxial strains of concrete along the first and second crack directions are again derived similarly. Steps described above for the first crack are similarly applied for the membrane model having two cracks formed. Compression softening and biaxial damage parameters are again considered in this step. Similar to the previous step, stress values for reinforcing steel bars are calculated and superimposed with the softened concrete stress to obtain panel element stress values. All three stages of panel responses are summarized in Figure 2.1 below.

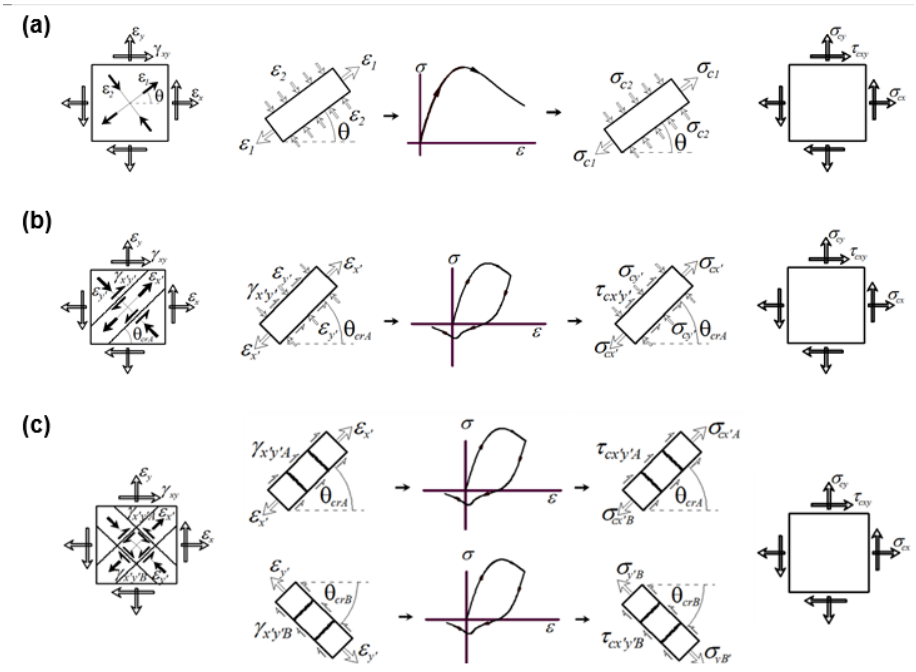

Figure 2.1. Concrete behavior in the Fixed Strut Angle Model: (a) uncracked, (b) after formation of first crack, (c) after formation of second crack.

2.2. Material Constitutive Models

State-of-the-art hysteretic material models and behavioral constitutive relationships that are existent in the original formulation of the FSAM by Ulugtekin (2010) are summarized herein. Some of these relationships also simulate physical observations such as biaxial damage on concrete, tension stiffening or compression softening in concrete.

2.2.1. Constitutive Material Model for Concrete

The uniaxial nonlinear hysteretic model (Figure 2.2) first developed by Chang and Mander (1994) was implemented in the FSAM formulation as it considers critical behavioral characteristics of concrete such as hysteretic behavior under cyclic compression or tension, impacts of gradual crack closures or tension stiffening and progressive stiffness degradation with the incremented strains under loading. Model proposed by Chang and Mander is an enhanced, generalized, and non-dimensional model which makes it feasible to simulate the hysteretic behavior of concrete with different features (e.g. confined, unconfined and standard/higher strength concretes both in tension and compression).

In the Chang and Mander model (1994), envelope for the stress strain relationship is defined by a monotonic curve and the concrete under tension is described similar to the cyclic behavior in compression. Slope of stress-strain behaviour at the origin as well as the shape before and after peak stress are all controlled by the model envelopes for tension and compression. Model needs to be carefully calibrated as shape of the envelopes can be modified while keeping the peak stresses and corresponding strains fixed. Chang and Mander (1994) used the widely accepted formulations derived by Tsai (1988) for defining the compression and tension envelopes.

For derivation of the cyclic parameters of concrete under compression, Chang and Mander (1994) carried out a set of statistical regression analyses on a large dataset. The analyses carried out using the large dataset, including experimental results available in

the literature (e.g. Sinha *et al.* (1964), Karsan and Jirsa (1969), Spooner and Dougill (1975), Okamoto *et al.* (1976) and Tanigawa and Uchida (1979)), allowed Chang and Mander (1994) to derive a set of empirical relationships for main hysteretic parameters (e.g. stress and strain offsets at compression envelope, secant and plastic stiffness during unloading).

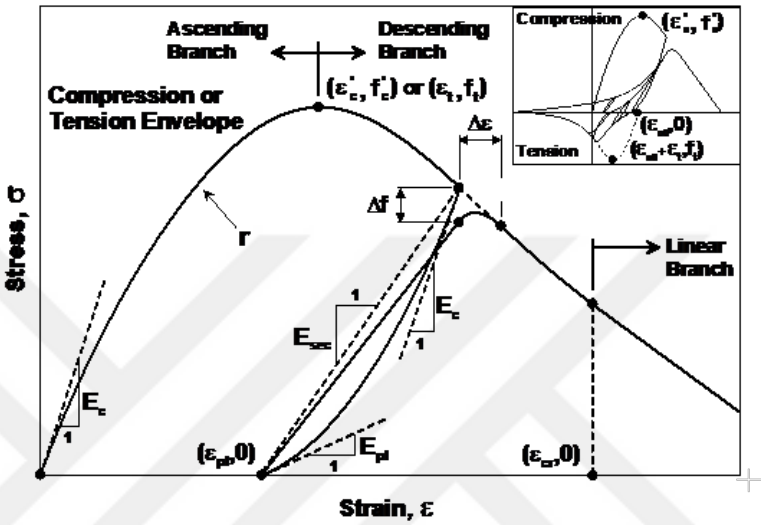

Figure 2.2. Constitutive Material Model for Concrete (Chang and Mander 1994).

2.2.2. Constitutive Material Model for Steel Reinforcement

The uniaxial stress strain relationship for reinforcing steel bars developed by Menegotto and Pinto (1973) and extended by Filippou *et al.*, (1983) to incorporate isotropic strain hardening was implemented in the FSAM for being a practical yet accurate constitutive material model. As shown in Figure 2.3, the stress strain relationship proposed by Menegotto and Pinto (1973) is not linear during the cyclic loading as reversal points are connected by curved lines. These curved lines are bounded by two straight line asymptotes, one being a straight line with a slope of Eo (modulus of elasticity) and the other being a straight line with a slope of E1 (yield modulus). Strain hardening ratio (b) is also represented as follows:

$$b = \frac{E_1}{E_o} \tag{2.9}$$

As these two asymptotes are connected using curves rather than linear lines, a shape parameter for defining the curvature is also defined. The curvature parameter (R) calculated by the following equation is also employed for reflecting the Bauschinger's effect.

$$R = R_0 - \frac{a_1.\xi}{a_2 + \xi} \tag{2.10}$$

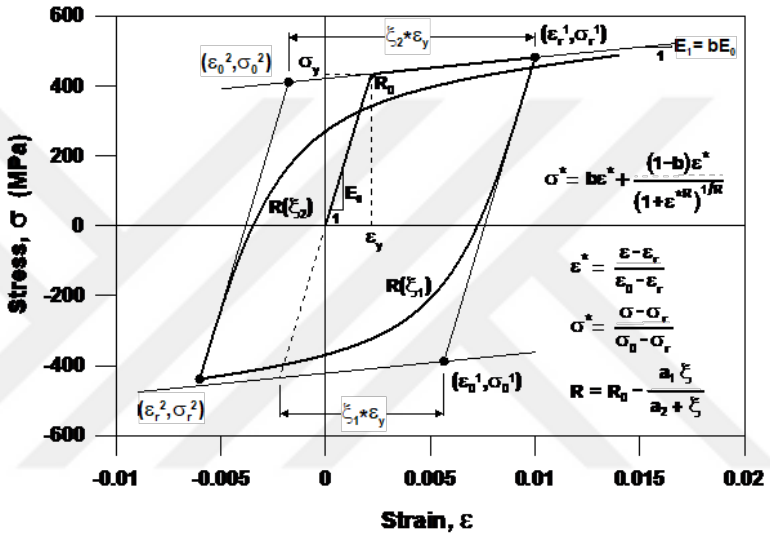

Figure 2.3. Constitutive Material Model for Reinforcing Steel (Menegetto and Pinto 1973).

2.2.3. Compression Softening of Concrete

Based on experimental observations of researchers, like Vecchio and Collins (1986), a reduction factor for the compressive stresses in concrete across the principal compression directions of reinforced concrete panel elements was introduced for modeling purposes. This compression softening phenomenon resulted from the tensile strains which occur along perpendicular principal directions. Other researchers (e.g., Vecchio and Collins 1993 and Belarbi and Hsu 1995) also reduced the strain value corresponding to the peak compressive stress. Despite the fact that most of these constitutive models were employed for monotonic loading conditions, they were also used in various cyclic analysis methods (e.g. Vecchio and Collins 1993 or Belarbi and Hsu 1995).

Although more complex models were proposed by researchers such as Vecchio and Collins (1993) ("Model A") or Belarbi and Hsu (1995), a simpler yet reasonably accurate model, "Model B" (Vecchio and Collins, 1993), was implemented to FSAM's formulation. "Model B" is simpler because it only reduces the peak compressive stress (Figure 2.4), whereas "Model A" by Vecchio and Collins (1993) or mode by Belarbi and Hsu (1995) modifies both the peak compressive stress and the corresponding strain values.

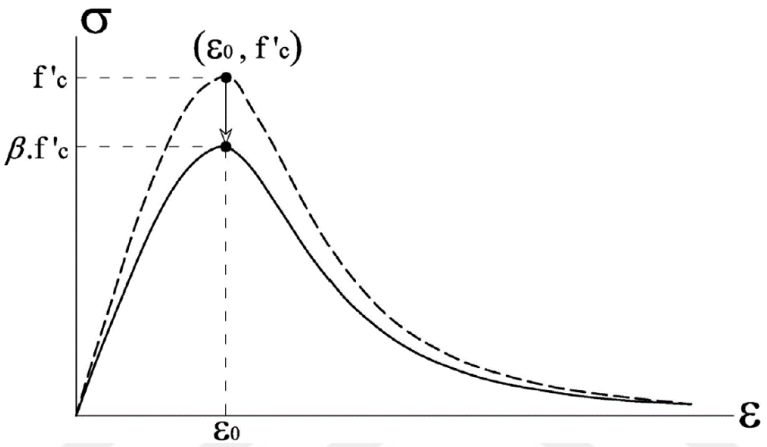

Figure 2.4. Compression Softening Effect based on Model B (Ulugtekin 2010).

2.2.4. Tension Stiffening Effect on Concrete and Steel

With cracking of concrete, a physical phenomenon called the tension stiffening may be observed, usually caused by the concrete that still surrounds the reinforcing bars which increases the tensile resistance of the cracked element. As implied by its definition, tension stiffening is effective in the post-cracking behavior of concrete as well as on yield capacity, shear characteristics and post-cracking stiffness, as demonstrated by researchers; Vecchio and Collins (1988), Stevens (1987), Collins and Mitchell (1991), Belarbi and Hsu (1994), Pang and Hsu (1995), Hsu and Zhang (1996), Mansour *et al.*, (2002), Hsu and Zhu (2002).

As can be seen in the upcoming sections of this thesis, two set of experimental programs were used for testing the model results. In order to validate the FSAM, two alternative tension stiffening models were implemented. Tension stiffening model

proposed by Stevens (1987) used for capturing the responses of the specimens used in the researcher's study whereas tension stiffening model proposed by Belarbi and Hsu (1994) employed for simulating the responses of the specimens tested by Mansour and Hsu (2005). Model proposed by Stevens (1987) assumes the average tensile stress-strain behavior of concrete as linear until cracking, and after cracking evolving into an exponential curve. In the model proposed by Belarbi and Hsu (1994) (Figure 2.5), similar to Stevens (1987), the average tensile stress-strain behavior of concrete is assumed to be linear until cracking, however, a descending curve is assumed.

Model proposed by Belarbi and Hsu also differentiates the average stress strain relationships of bare bars from bars surrounded by concrete (Figure 2.6). Main differences can be summarized as: (i) reducing the yield stress after steel stress (cracking section) surpasses yield strength of the bare bar and (ii) lowering the average shear stress distributed along the element compared to the yield stresses of the bare bars. RC panel experiments and data collected from those experiments demonstrate that the diminished yield stresses (effective yield stress) of bars surrounded by concrete can be linked empirically to the cross-sectional area of longitudinal reinforcement, concrete cracking stress to steel yield stress ratio and steel elastic modulus to concrete elastic modulus ratio.

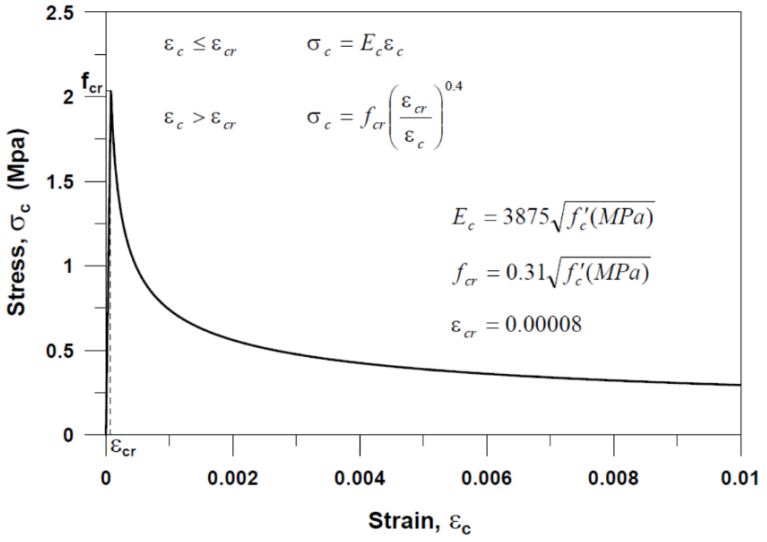

Figure 2.5. Average stress-strain relationship by Belarbi and Hsu (1994) for concrete in tension.

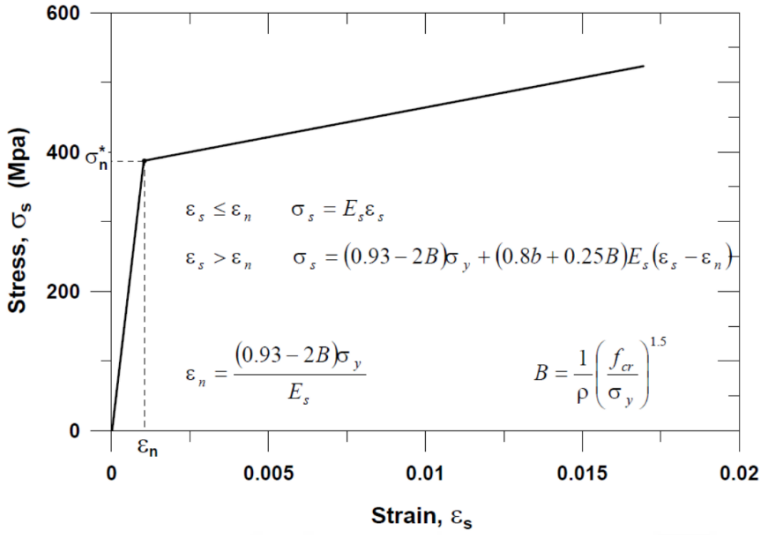

Figure 2.6. Average stress-strain relationship by Belarbi and Hsu (1994) for reinforcing bars embedded in concrete.

The reason that two different constitutive models for tension stiffening were used in the formulation for comparison of model results with test results is that the tension stiffening model is not a unique attribute of the. The researchers (Mansour (2001) and Stevens 1987) who conducted the panel tests considered in this study (for experimental validation of the) have stated that the two tension stiffening models (Hsu 1994 and Stevens 1987) best represent the experimentally observed of their test specimens. Therefore, the was experimentally validated for the two respective test programs, with the two respective tension stiffening models in its formulation, for a more consistent evaluation of its performance.

2.2.5. Biaxial Damage on Concrete

Impacts of cyclic damage on concrete subjected to biaxial loading is also taken into account in the FSAM formulation, which also improves the model formulation by considering another critical behavioral phenomenon. Similar to compression stiffening parameter, cyclic damage on concrete subjected to biaxial loading is applied by a damage coefficient. However, since this coefficient is a cyclic-strain-history-dependent parameter, it is not used in the analysis of reinforced concrete membrane elements sub-

jected to monotonic loading. This coefficient is only valid for biaxial loading situations as it is a parameter that considers the impacts of recorded or historical compressive strains perpendicular to compressive stress directions along compression struts.

Similar to the approach used for incorporating tension stiffening in the FSAM, two alternative empirical models available in literature for the damage coefficient were implemented in the formulation of the FSAM for the experimental validation studies presented in this paper; one by Stevens (1987) (used for comparison of model results with tests by Stevens, 1987), and the other by Mansour *et al.*, (2002) (used for comparison of model results with tests by Mansour, 2001). It should be mentioned that using the two different biaxial damage coefficients in the formulation of the FSAM did not result in significant differences in model results obtained for all panel specimens investigated in this study. Details of these biaxial damage parameters are presented in the study by Ulugtekin (2010).

2.3. Nonlinear Analysis Solution Procedure

The FSAM formulation which is improved in this study to consider shear stress transfer across cracks was implemented in Matlab (2012) with a nonlinear displacement-controlled solution strategy for conducting analysis of reinforced concrete panel elements. An interpretation of the "arch-length" method with a displacement based iterative procedure (Clarke and Hancock 1990, Simons and Powell 1982) was followed.

Briefly, the solution approach can be explained in two main parts, first one is the "incrementation stage" and the second one is the "equilibrium stage". Incrementation stage is used for loading the system while the equilibrium stage is used for satisfying the equilibrium conditions between internal and external forces related to the imposed conditions. The solution strategy employed is presented in Figure 2.7 and Figure 2.8.

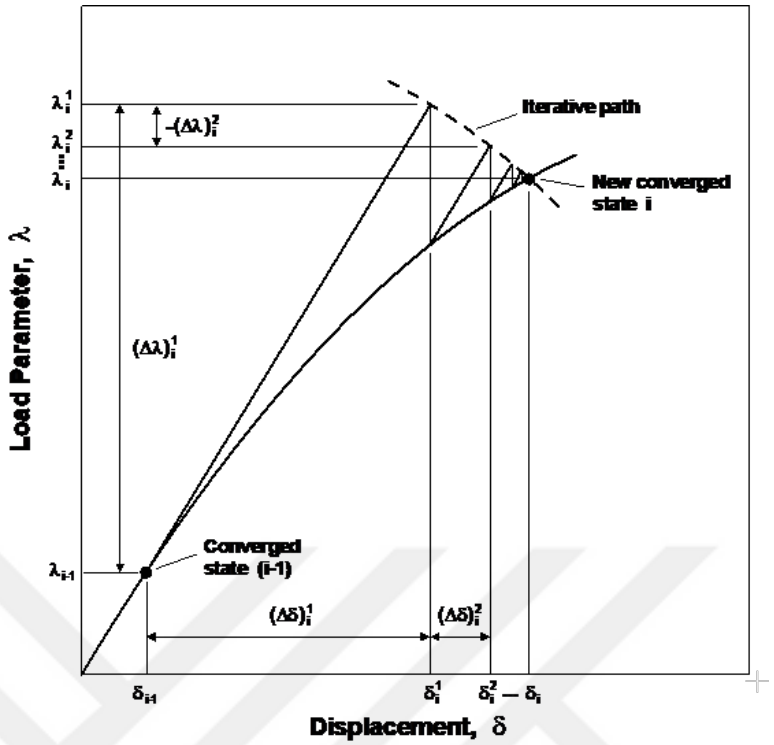

Figure 2.7. Representation of the Nonlinear Analysis Solution Strategy for a Single Degree of Freedom System (Clarke and Hancock, 1990).

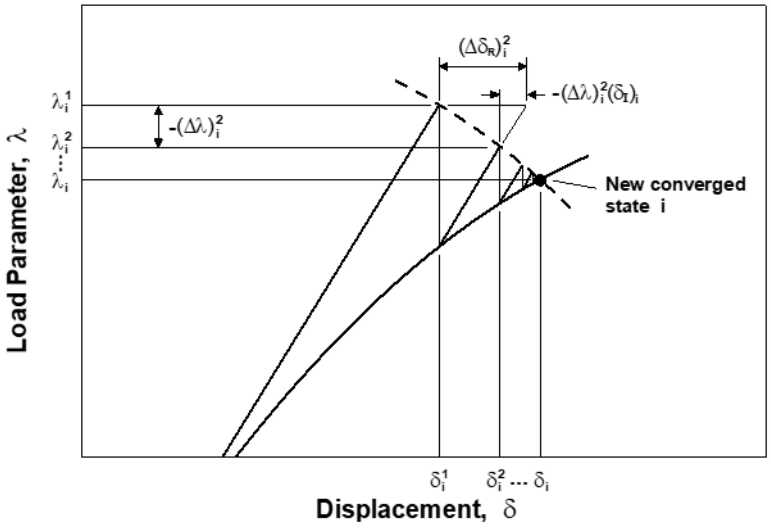

Figure 2.8. Iterative Strategy and Residual Displacements (Clarke and Hancock, 1990).

3. MODEL IMPROVEMENT THROUGH IMPLEMENTATION OF SHEAR RESISTING MECHANISMS ACROSS CRACKS

Improvements made on the constitutive panel model aims to better simulate the behavior of RC panel elements subjected to generalized, in-plane, reversed-cyclic loading by incorporating behavioral models that account the originally neglected shear stresses along the crack surfaces. Such improvements are made by way of introducing certain behavioral responses, which are friction based shear aggregate interlock ($\tau_a gr$), dowel action on reinforcing steel bars (τ_D) and the degradation of these shear resistance mechanisms due to cyclic loading conditions (i.e. cyclic degradation). After superimposing the resultant stresses (which occur due to shear transfer mechanisms incorporated) with the concrete stresses developing along the crack directions, as shown in Equation 3.1, model is expected to yield more accurate results and demonstrate the impacts of accounting such behavioral features.

$$\tau_{total} = \tau_{agr} + \tau_D \tag{3.1}$$

One of the main assumptions made in the FSAM formulation was the alignment of principal stress directions in concrete with the crack directions, implying that shear stresses along cracks were zero, and contribution of shear aggregate interlock was neglected. Shear aggregate interlock response is dependent on crack width and the amount of slip deformation across crack surfaces and it occurs due to sliding across crack surfaces. Additionally, dowel action on reinforcing steel bars also have an impact on the overall behavior and response predictions of the model. Degradation of these resultant shear stress contributions caused by cyclic behavior or loading conditions should also be considered. Results of the studies conducted by Ulugtekin (2010) demonstrates that neglecting shear aggregate interlock had an impact on shear stress capacity predictions of the FSAM. Although results were still in an acceptable range,

model underestimated shear capacity between 10%-20% (Ulugtekin 2010) for each of the specimens investigated. As interpreted from the results of sensitivity analyses, which are further explained in Section 4.3., it is also observed that the zero-aggregate interlock assumption in FSAM formulation leads to exaggerated shear strains along cracks for panel specimens with asymmetrical or inclined reinforcements.

3.1. Shear Aggregate Interlock Model

Under the impact of external loading conditions or due to existence of reinforcing bars intersecting the cracks, normal stresses acting on the crack interfaces results in shear transfer via friction. As shown in Figure 3.1, when the crack interface subjected to shear displacement (s), deformations along the surface leads to frictional stress. These deformations result in increase of the crack openings (w), which is restricted by the reinforcing bars having response with a tensile force (σ_s.As). Due to the equilibrium equations, tensile force is balanced by a counter-reacting force (i.e. compressive force or Ac.σ_c) on the concrete close to the rebar. Normal compressive stress applied perpendicular to crack surface and influence of the transverse reinforcement to the shear aggregate interlock mechanism is demonstrated in Figure 3.1. Researchers realized the need for a shear transfer mechanism that can capture this physical phenomenon and they have carried out extensive and various studies on this subject. One of these studies was carried out by Tassios *et al.*, (1987) in the National Technical University of Athens, where numerous experiments were carried out under monotonic or cyclic shear displacements for different types of crack interfaces (i.e. smooth vs. rough) in plain concrete to investigate their responses. Vintzeleou and Tassios (1987) also indicated that impact of cyclic loading on dowel response can be considered by adopting the relationships proposed for monotonic loading.

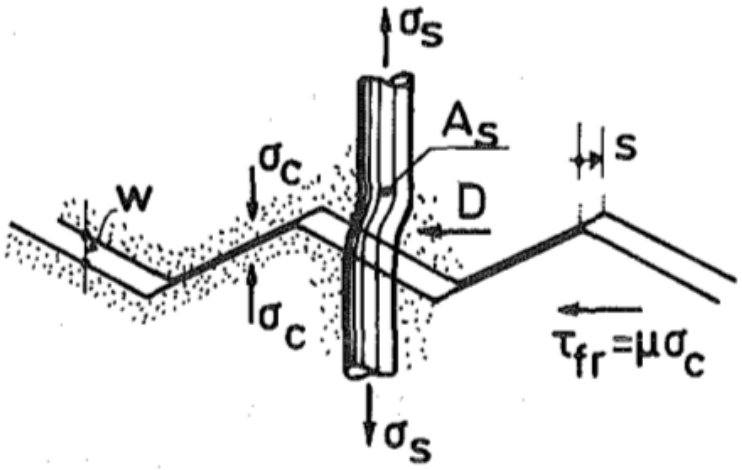

Figure 3.1. Qualitative Description of Friction Resistance, tau fr, besides Dowel Resistance, D (Tassios *et al.*, 1987).

Tassios *et al.*, (1987) suggested that normal compressive stresses applying along the crack surfaces and the contribution of the transverse reinforcement to the shear resistance along cracks significantly differentiate depending on the types of crack surfaces. As smooth surfaces are less inuous or wavy, only smaller granules are existent along the crack surface, hence dilatancies perpendicular to crack direction, if any, are not substantial. In other words, regardless of the intensity of the applied displacement, contribution of transverse reinforcements to shear resistance as described above does not work on these types of surfaces. However, as aggregates that are sticking out of the crack surfaces lead to interlock in rough surfaces, higher lateral dilatancies are observed in crack surfaces with rough interfaces under shear displacements. As it is explained in the previous paragraph, this would result in tensile forces along the rebars and depending on the degree of the resultant stress, contribution of transverse reinforcement to frictional resistance could be a significant portion of the total resistance in these types of surfaces. Moreover, a rough interface subjected to an external compression force inherently provides higher shear resistance as more particles or aggregates interlocks together with the additional compression.

In the paper by Tassios *et al.*, (1987), impact of different types of surfaces to the shear aggregate interlock mechanism were explained. Main observations were related

to modes of deterioration and failure mechanisms of specimens according to smooth and rough surfaces. Several parameters were scrutinized under the research program including interface types (rough: natural, smooth, sand-blasted: obtained by sand blasting of rough surfaces), concrete compressive strength and loading history. Test results and observations stated by Tassios *et al.*, (1987) are discussed within the scope of this thesis. Cyclic test results provided by Tassios *et al.*, (1987) for different interface types are summarized below:

(i) Smooth surfaces: Except for the test having normal stress value of 2.0 MPa, test results decreased by 30% in the second loading direction (Figure 3.2a) whereas the same response was observed in both loading directions when normal stress was kept at 2.0 Mpa. Cyclic degradation was not considerable (Figure 3.2a) compared to degradation in response for other surface types, implying that the smooth interface remained smooth during the entire loading history. In addition, no pinching effect was observed, and hysteresis loops were quite large. Observed crack openings were very small (< 0.2mm) although width of these cracks were increasing throughout the loading steps (Figure 3.2b), explained by the left-over particles (that were torn from the surface but still remained along crack surface) that blocks the interface.

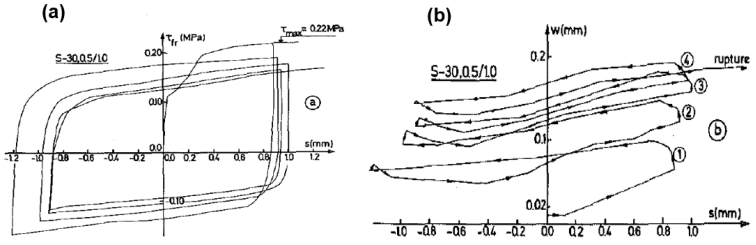

Figure 3.2. (a) Typical Hysteresis Loops for Smooth Interfaces Subjected to Full Slip Reversals; (b) Typical Dilatancy vs. Shear Displacement Diagram for Cyclically Loaded Smooth Interfaces (Tassios *et al.*, 1987).

(ii) Rough surfaces (including sand blasted surfaces): Unlike the smooth surfaces, response in the second loading direction was observed to be significantly lower than of first loading direction, leading to asymmetry in the hysteresis loops (Fig-

ure 3.3a). In following cycles, decreases in response becomes relatively marginal. Crack dilatancy vs. slip deformation results for rough surface is presented in Figure 3.3b. As shown in Figure 3.3a, following the loading reversals shear stiffness decreases significantly and considerable pinching effect is observed in the hysteresis loops. Residual slip deformation after unloading is almost same since maximum shear slip for each loading cycle after unloading and the surface is not rough anymore. In contrary to smooth surfaces, the cyclic degradation was significant as the aggregates that interlock the crack surface smoothen or deteriorate, especially in first cycles where the deterioration of rough surfaces are considerable compared to subsequent cycles. As a result of severe cyclic degradation, the lateral dilatancies and the crack width decreased as well (Figure 3.3b). It was also revealed that cyclic degradation was a function of (a) normal stress applied perpendicular to the crack surfaces and (b) maximum shear displacement applied to the specimens.

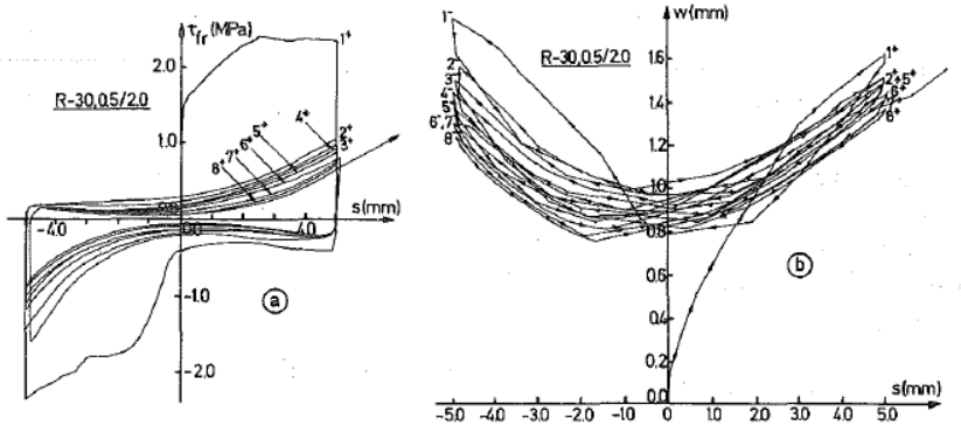

Figure 3.3. (a) Typical Hysteresis Loops for Rough Interfaces Subjected to Full Slip Reversals; (b) Typical Dilatancy vs. Shear Displacement Diagram for Cyclically Loaded Rough Interfaces (Tassios *et al.*, 1987).

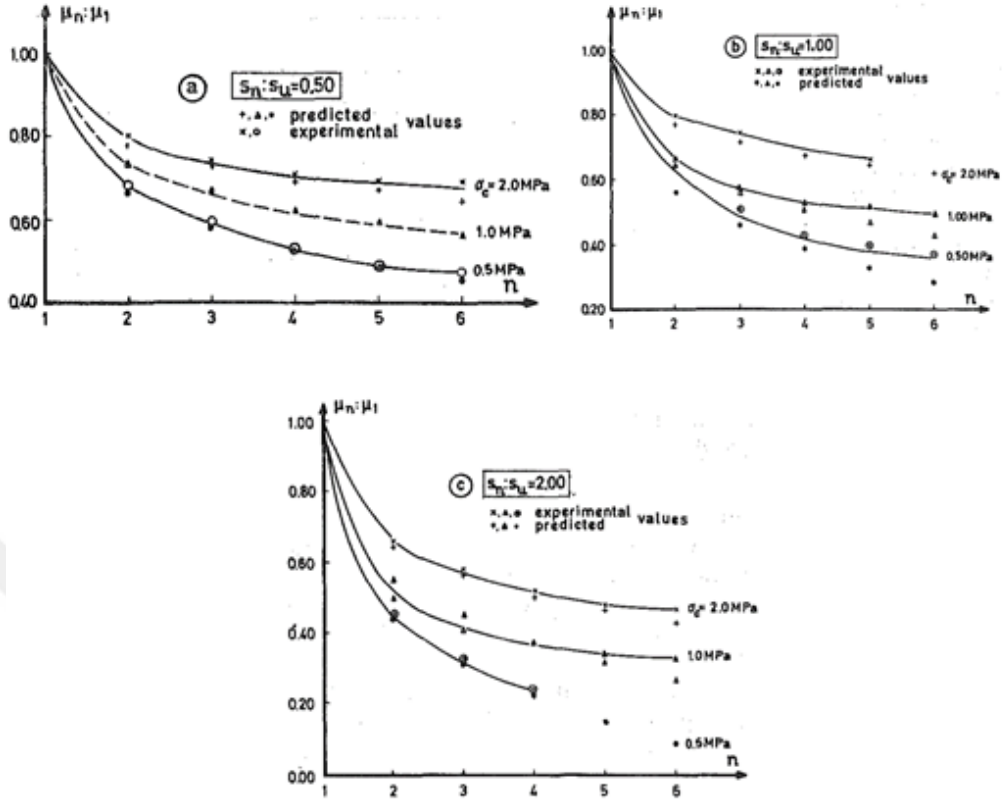

Figure 3.4. Rough Interfaces: Decrease of Maximum Friction Coefficient Due to Cycling as Function of Normal Stress and for Several Normalized Displacement Ratios (sn/su) (Tassios *et al.*, 1987).

Based on the test results summarized above, empirical models that are applicable for both surface types under monotonic and cyclic loading conditions were proposed by Tassios *et al.*, (1987). Degradation parameters for rough (Figure 3.4) and smooth interfaces (Figure 3.5) are presented herein. For rough interface degradation parameter in shear stress capacity is calculated by the following equation: where $\tau_(fr,1)$ is not fixed and could be any shear stress (friction) observed under σ_c.

$$\tau_{fr,n} = \tau_{fr,1}\left\{1 - \left[0.002\,(n-1)\left(\frac{\sigma_c}{f_{cc}}\right)^{-1}\left(\frac{s_n}{s_u}\right)\right]^{1/3}\right\} \tag{3.2}$$

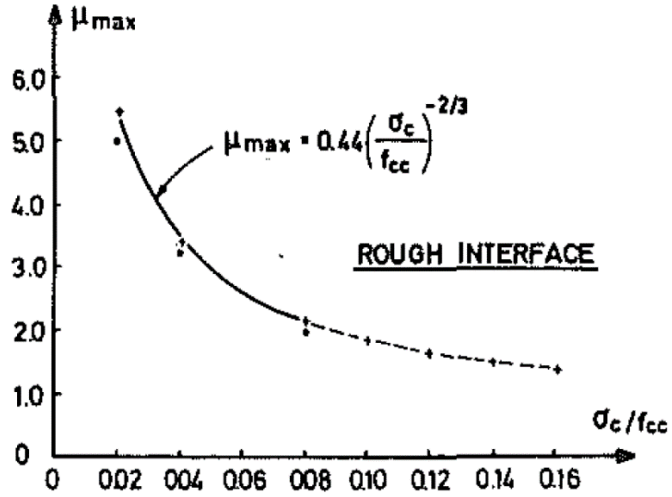

Figure 3.5. Maximum Friction Coefficient for Rough Interfaces as Function of Normal Stress Normalized to Concrete Compressive Strength (Tassias *et al.*, 1987).

Cyclic degradation parameters for shear stress in smooth interface is given by:

$$\tau_{fr,n} = \tau_{fr,1}\left(\frac{1}{7}\sqrt{n-1}\right); if s_n > s_u \tag{3.3}$$

where

$$\tau_{fr,1} = 0.40\sigma_c \tag{3.4}$$

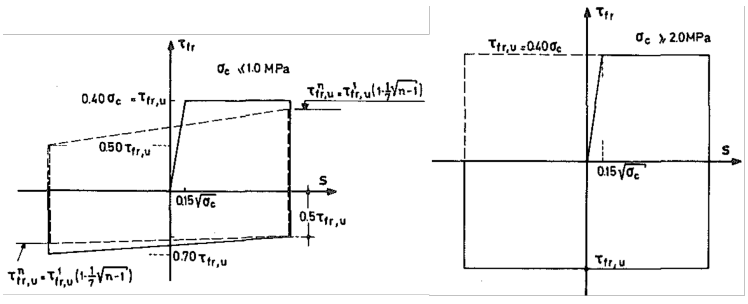

Figure 3.6. Formalistic Models for Shear Transfer Against Smooth Interfaces Subjected to Cyclic Actions: (a) For Low Normal Stresses; (b) for High Normal Stresses Acting on Interface (s in mm and σ_c in MPa) (Tassios *et al.*, 1987).

Based on the study by Tassios *et al.*, (1987), original FSAM formulation was first extended by Orakcal *et al.*, (2012) by incorporating a simple friction-based aggregate interlock constitutive model (Figure 3.6). As can be seen in Figure 3.6, adopted friction-based aggregate interlock model proposed by Orakcal *et al.*, (2012) relates the sliding shear strain ($\gamma'_x y'$) to the resultant shear stress ($\tau'_x y'$) by an elasto-plastic model, similar to test results provided by by Tassios *et al.*, (1987) for smooth interfaces. However, cyclic degradation parameters were not employed in the study by Orakcal *et al.*, (2012). Model for friction-based shear aggregate interlock demonstrating elasto-plastic behavior under constant compressive stress ($\sigma_{\perp c}$=constant) as shown in Figure 3.6 is similar to reinforcing steel model. As shown in Equation 3.4, the initial slope of the elasto-plastic strain vs. stress curve was equal 0.4 times the elastic shear modulus of concrete ($E_(c)$).

$$G_C = 0.4.E_c \tag{3.5}$$

It is important to mention that when the concrete normal stress perpendicular to the crack direction is tensile, in other words if the crack is open as shown, the resultant shear stress becomes zero. However, when the normal stress turns into compression (crack is closed), the shear stress becomes a value calculated as shown in Equation 3.5 below, which is related to the friction coefficient(η).

$$\tau_{x'y'} = \eta.\sigma_{\perp c} \tag{3.6}$$

The friction coefficient may vary for each of the specimens based on their physical properties (e.g. reinforcement alignments and ratios) or test setup (e.g. loading conditions). Sensitivity studies for the improved model to the friction coefficient is conducted with further details in the next chapter (Chapter 4). Specimens were calibrated with their optimum friction coefficients, which are derived in Section 4.3. According to calibrated friction coefficients for each of the specimen model predictions were compared against test results in the following sections of the same chapter (Chapter 4,

Section 4.4 and Section 4.5).

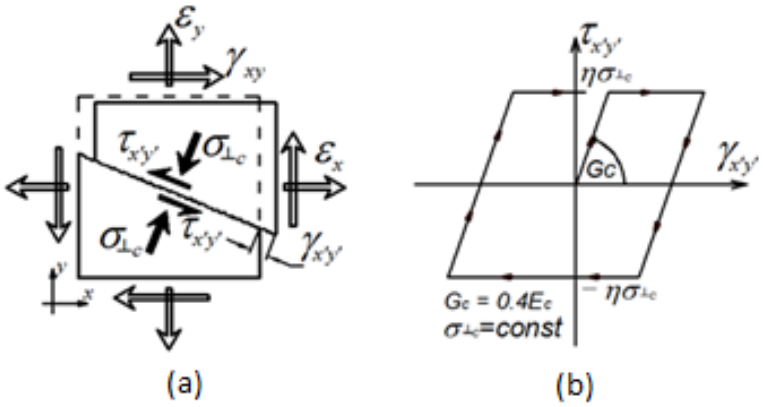

Figure 3.7. (a) Strains and stresses along a crack, (b) Friction-based constitutive model for contribution of concrete stress to aggregate interlock (Gullu and Orakcal, 2017).

3.2. Dowel Action Model on Reinforcing Bars

Second improvement was the incorporation of dowel actions for both horizontal and vertical rebars via implementation of a simple origin-oriented relationship in the form of a monotonic envelope of the dowel stress vs. strain as proposed by He and Kwan (2001). Reason for implementing an origin-oriented model with the monotonic envelope by He and Kwan (2001) lies in its simplicity. The proposed modeling approach in the study by He and Kwan (2001) allows easy integration to another analytical models as it was derived on a smeared crack approach making it compatible with most membrane models available in the literature.

As illustrated in Figure 3.7a, distortion of reinforcing bars leads to transverse shear forces and contra-flexural bending moment, as concrete blocks slide in reverse directions. He and Kwan (2001) formulates the dowel deformation and the dowel force as follows:

$$\Delta_{dow} = l.\gamma_{xy} \tag{3.7}$$

$$V_d = K_d.\Delta_{dow} \tag{3.8}$$

where K_d is the secant stiffness for dowel model of the reinforcing bar. Effective dowel length l in the equation above is calculated as:

$$l = \frac{\pi}{\lambda} \tag{3.9}$$

where

$$\lambda = \sqrt[4]{\frac{k_c d_b}{4E_s I_s}} \tag{3.10}$$

In equations above, Es represents the modulus of elasticity for steel, I_s represents the moment of inertia of the bar, λ represents relative stiffnes of the foundation and kc is the foundation modulus of the surrounding concrete.

In the paper by He and Kwan (2001) every reinforcing bar was assumed as a separate beam by implementing the "beam on elastic foundation" theory proposed by Hetenyi (1958). The theory proposed by Hetenyi (1958) suggested that the foundation could be treated as a bed of Winkler springs (Figure 3.7b), meaning that at any selected point along the foundation, the reacting forces are proportional to the deflection.

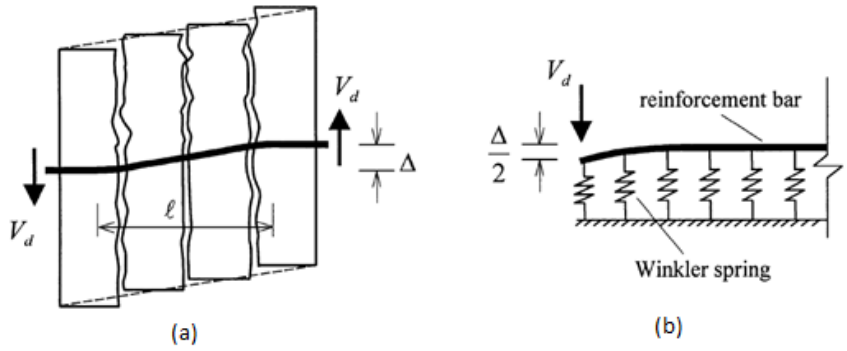

Figure 3.8. (a) Analysis of dowel action using "beam on elastic foundation" theory (He and Kwan 2001).

If half the bar from the cross section where contra-flexion was observed is considered, it is reasonable to treat the bar as a semi-infinite beam with force (Vd) acting on one end. Solving the beam analytically for a beam on an elastic foundation, the following value is obtained:

$$V_d = E_s I_s \lambda^3 \Delta_{dow} \tag{3.11}$$

Before reaching the capacity of the dowel model, dowel force-displacement relationship is considered to be linear elastic whereas this relationship turns into plastic upon reaching capacity. Once the capacity is reached, the surrounding concrete crushes locally and/or the reinforcing bars start yielding. Tests carried out by Dulacska (1972) resulted with the following relationship for estimating the dowel force capacity:

$$V_d = 1.27 d_b^2 \sqrt{|f'_c|\,|f_y|} \tag{3.12}$$

In addition, using the "smeared" stress approach, dowel stress is smeared across the crack surface, and represented as follows:

$$\tau_{xy}^d = \frac{\rho_s}{A_S}.\mathrm{V}_d \tag{3.13}$$

where ρ_s and A_S represent the reinforcement ratio in crack direction and the sectional area of reinforcement, respectively. In cases where the reinforcing bars are not along the principal axes, following equation are used to obtain the tensile and shear stresses across the cracks.

$$\begin{bmatrix} \sigma_1^d \\ \tau_{12}^d \end{bmatrix} = [T_d]^t \begin{bmatrix} \frac{\rho_x}{A_{sx}} K_{dx} l_x & 0 \\ 0 & \frac{\rho_y}{A_{sy}} K_{dy} l_y \end{bmatrix} [T_d] \begin{bmatrix} \varepsilon_1 \\ \gamma_{12} \end{bmatrix} \tag{3.14}$$

where

$$[T_d] = \begin{bmatrix} \cos\theta \sin\theta & \cos^2\theta \\ \cos\theta \sin\theta & -\sin^2\theta \end{bmatrix} \tag{3.15}$$

The presented dowel action model is similar to the model proposed by Vintzeleou and Tassios (1987) and was also used in the improved FSAM to estimate the dowel force reaching (Figure 3.8a). The results of the tests carried out by Dei Poli *et al.*, (1992), Dulacska (1972) and Vintzeleou and Tassios (1987) suggests that the relationship between the dowel force and displacement could be interpreted as linear elastic before reaching capacity.

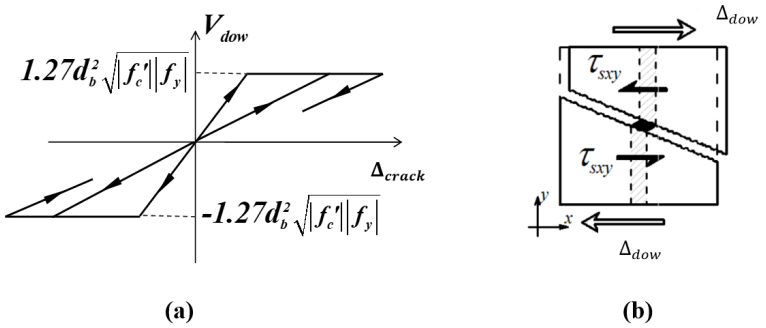

Figure 3.9. (a) Dowel action model (b) Illustration of dowel action.

Cyclic degradation parameters for aggregate interlock effects may increase the contribution of dowel action within the global shear transfer mechanism, also effecting the response of the panels. Absence of dowel action model in the FSAM formulation may have a significant impact on the global and local results. As shown in Figure 3.9a, parameters like bar diameter, material strengths, reinforcement ratio and effective dowel length were used to define the empirical dowel strength and stiffness values. Based on the detailed studies available in the literature, hysteretic rules were also defined as origin-oriented, for simplicity in hysteretic dowel action model formulation.

3.3. Cyclic Degradation Parameters

Final improvement to the FSAM was conducted by introducing cyclic degradation parameters for the shear aggregate interlock and dowel action models. Cyclic degradation parameters incorporated in the FSAM originated from cyclic constitutive degradation relationships developed by Vassilopoulou and Tassios (2003), which is based on the studies by Tassios and Vintzileou (1986) for dowel action and Tassios and Vintze-leou (1987) for shear aggregate interlock. Cyclic degradation parameters were

linked to the number of cycles employed throughout the entire loading history (Figure 3.10). This original model was further extended by Thermou *et al.*, (2014), including the introduction of an arbitrary number for cycles which shifted the dependency of the model from actual number of cycles to cumulative and maximum slip.

$$n_{eq} = \frac{1}{4}\left(\frac{\sum^{s}}{|s_{max}|} + 1\right) \tag{3.16}$$

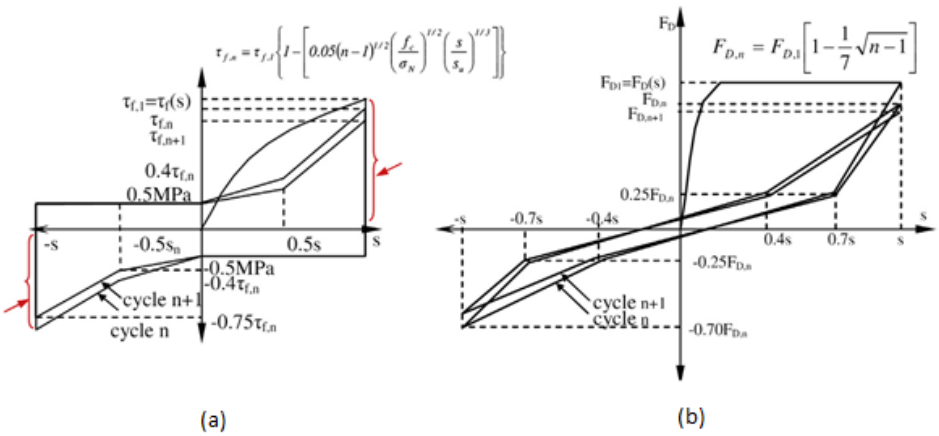

Figure 3.10. Response to symmetric cyclic loading: (a) friction and (b) dowel (Thermou *et al.*, 2014).

Implementing the number of cycles in the cyclic degradation equations in Figure 3.10, cyclic degradation parameters were finally adopted in this study for shear aggregate interlock and dowel action models as shown in equations below. The parameters in the equations below are as follows: Σ_{Δ} representing total slip deformation, s_{max} representing the maximum slip deformation, Δ_{max} representing the degradation parameter (as introduced in Greek Code of Interventions (KAN.EPE) 2013) and Δ_u equals to 2mm.

$$\tau_{\mathrm{crack,deg}} = 1 - 0.05\alpha\sqrt{\frac{\Sigma\,\Delta\,/\,|\Delta_{\mathrm{max}}| + 1}{4}}\left(\frac{f'_c}{\sigma_{c\perp}}\right)^{1/2}\left(\frac{|\Delta_{\mathrm{max}}|}{\Delta_u}\right)^{1/3} \tag{3.17}$$

$$V_{\mathrm{dow,deg}} = 1 - \alpha \frac{1}{7} \sqrt{\frac{\Sigma \Delta / \Delta_{max} + 1}{4}} \tag{3.18}$$

Since cyclic degradation parameters are defined based on the stress vs. strain relationship, in the formulation of the FSAM, shear strains are modified to shear deformations across the crack interface. Shear strains (γ_{crack}) developed along crack surface are multiplied with the calculated nominal crack spacing (s), as defined in the papers by Vecchio and Collins (1986) and Vecchio (2000), to obtain slip deformations at the crack interface. Slip deformation along the crack interface and related nominal crack spacing is calculated by the following equations:

$$\Delta_{crack} = \gamma_{crack}\, s \tag{3.19}$$

$$s = \frac{1}{\frac{\sin\theta}{s_x} + \frac{\cos\theta}{s_y}} \tag{3.20}$$

where θ is the crack angle, and s_x and s_y are defined as the distance between horizontal reinforcing bars and vertical reinforcing bars, respectively.

Figure 3.11 and Figure 3.12 show the constitutive cyclic relationships finally adopted in this study for shear aggregate interlock and dowel action mechanisms. In Figure 3.11, the origin-oriented hysteretic dowel action on reinforcements and cyclic degradation parameters reducing the shear stresses are presented. Friction-based shear aggregate interlock model with cyclic degradation parameters are illustrated in Figure 3.12.

The improved FSAM formulation, with the new constitutive models for shear aggregate interlock and dowel action mechanisms, was used to conduct the following parametric sensitivity studies, as well as for global and local comparisons between model predictions and test results on RC panel specimens. Validation of the improved model with test results is discussed in the following chapter.

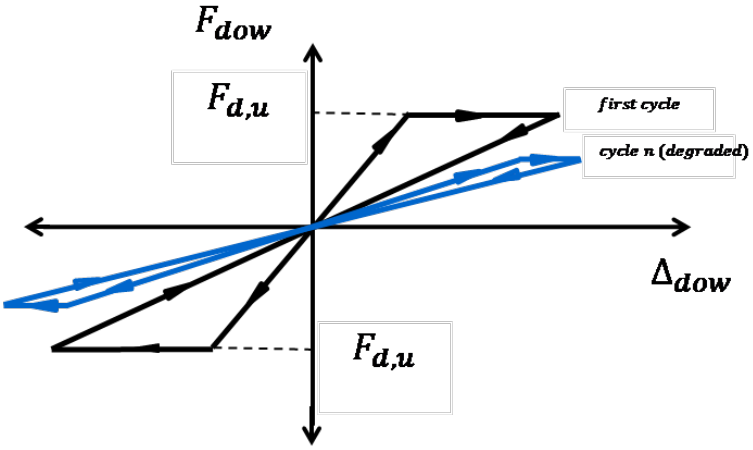

Figure 3.11. Implemented origin-oriented model for dowel action with cyclic degradation.

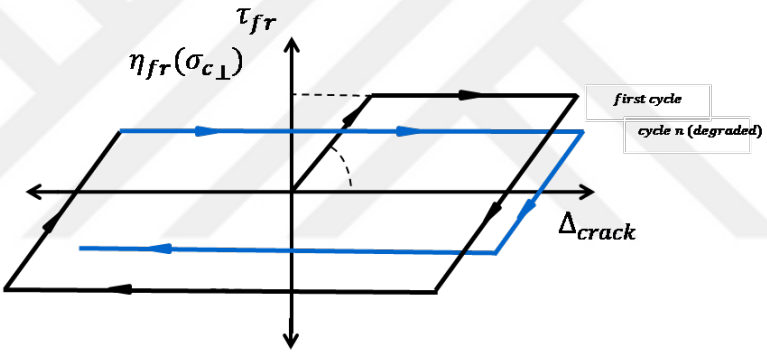

Figure 3.12. Implemented friction-based model for shear aggregate interlock with cyclic degradation.

4. COMPARISON OF MODIFIED MODEL RESULTS AND PARAMETRIC SENSITIVITY ANALYSES WITH EXPERIMENTAL PROGRAMS

Validation of the model against test results is presented in this chapter. Panel test specimens used for model validation are first described, thereon parametric sensitivity analyses conducted for the specimens sensitive to the coefficient of friction in the shear aggregate interlock model. and their results are discussed. Global and local response predictions of the model with the individual values of coefficient of friction for each of the panel specimens are also presented going forward.

4.1. Properties of panel elements tested by Stevens (1987)

All of the panel tests by Stevens (1987) were conducted under stress control. Test panels were square, with 1625x1625 mm dimensions and 285 mm thickness (Figure 4.1). The test equipment was configured for loading principal (normal) stresses on the panel specimens. All panel reinforcements were arranged orthogonally in x and y directions, with reinforcement ratios being ρ_z and ρ_y. Material properties, reinforcement ratios, and loading characteristics of the test program are listed in Table 4.1. In this experimental program, there were two different parameters investigated; the loading type and reinforcement ratio. While specimens SE8 and SE10 were used to examine the effect of loading type on panel response (pure shear stress applied on SE8 and SE9; shear stress with proportionally-applied normal stresses $\sigma_x = \sigma_y = -|\tau_{xy/3}|$ applied on SE10), specimens SE8 and SE9 were utilized to investigate the effect of reinforcement ratio on the response ($\rho_z = 0.03$, $\rho_y = 0.01$ for SE8 and SE10; $\rho_z = \rho_y = 0.03$ for SE9).

Table 4.1. Parameters of the panel elements tested by Stevens (1987).

Panel Specimen	**SE8**	**SE9**	**SE10**
Loading Type	σ_x=0 σ_Y=0 τ_{xy} : *Reversed Cyclic*	σ_x=0 σ_Y=0 τ_{xy} : *Reversed Cyclic*	$\sigma_x = -\lvert\tau_{xy/3}\rvert$ $\sigma_y = -\lvert\tau_{xy/3}\rvert$ τ_{xy} : *Reversed Cyclic*
ρ_x	0.03	0.03	0.03
ρ_y	0.01	0.03	0.01
$f_{y,x}[MPa]$	492	422	422
$f_{y,y}$***[MPa]***	479	422	479
f'_c***[MPa]***	37	44	34
ε_{co}	0.0026	0.0026	0.0023
f_{ct}***[MPa]***	2.0	2-Feb	2.0
ε_t	0.0001	0.0001	0.00013

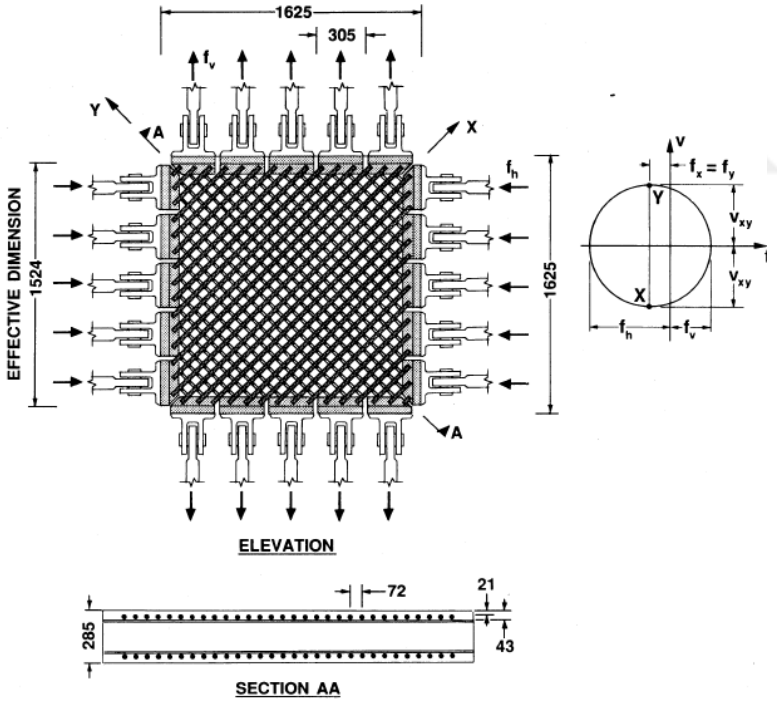

Figure 4.1. Specimen dimensions (mm) and application of stresses *et al.*, 1991).

4.2. Properties of panel elements tested by Mansour and Hsu (2005)

There are two important characteristics of the experimental program by Mansour (2005). First, these tests (12 full-size reversed cyclic panel tests) were performed under

strain control, which revealed the sudden stiffness drop as an effect of first cracking on panel response, as well as degradation in shear stress during later stages of loading due to the behavior of concrete in compression. Second, the test program was aimed to investigate the effect of reinforcement ratio to the overall behavior (i.e., $\rho_z = \rho_y =$ 0.0077 for CA2; $\rho_z = \rho_y = 0.017$ for CA3; $\rho_z = \rho_y = 0.027$ for CA4), asymmetry of reinforcement ratio in the orthogonal directions (i.e., $\rho_z = 0.017, \rho_y = 0.0077$ for CB3; $\rho_z = 0.027$, $\rho_y = 0.0067$ for CB4) and different loading conditions (i.e., pure shear stress on CA2, normal and shear stresses on CD4, and normal stresses on CE4).

The orientation of reinforcement was a test variable in this experimental program in order to generate the different loading conditions. Thus, a selection of 7 specimens (CA2, CA3, CA4, CB3, CB4, CD4, and CE4), among the total of 12, that capture the various test variables were considered within the scope of this study. All of these panel specimens had 1397x1397 mm dimensions and 178 mm thickness. The testing was configured for application of principal (normal) strains to the test specimens at different angles, resulting in pure shear stress (CA and CB series-reinforcement at 45° relative to external loading), in pure normal stresses (CE series - reinforcement parallel to external loading) and combined normal and shear stresses (CD series - X reinforcement at 68.2° relative to one of the external loading directions). Material properties, steel reinforcing ratios, and loading characteristics of the test specimens are described in Table 4.2 Figure 4.2 to Figure 4.4 illustrate dimensions and orientation of reinforcing bars for each panel series and Table 4.3 summarizes the reinforcement angles relative to the applied stress for each panel series tested by Mansour and Hsu (2005).

Table 4.2. Parameters of the panel elements tested by Mansour and Hsu (2005).

Panel Specimen	**CA2**	**CA3**	**CA4**	**CB3**	**CB4**	**CD4**	**CE4**
Loading Type	σ_x=0 σ_y=0 τ_{xy} : RC	σ_x=0 σ_y=0 τ_{xy} : RC	σ_x=0 σ_y=0 τ_{xy} : RC	σ_x=0 σ_y=0 τ_{xy} : RC	σ_x=0 σ_y=0 τ_{xy} : RC	σ_x=1.05 τ_{xy} σ_y=1.05 τ_{xy} τ_{xy} : RC	σ_x=RC σ_y= $-\sigma_x$ τ_{xy}=0
ρ_x	0.0077	0.017	0.027	0.017	0.027	0.02	0.019
ρ_y	0.0077	0.017	0.027	0.0077	0.0067	0.02	0.019
$f_{y,x}$ *[MPa]*	424	425	453	425	453	453	453
$f_{y,y}$ ***[MPa]***	424	425	453	424	424	453	453
f'_c ***[MPa]***	45	44.5	45	48	47	43	47
ε_{co}	0.0025	0.0024	0.0028	0.0026	0.0024	0.0024	0.0022
f_{ct} ***[MPa]***	2.2	2.2	2.2	2.2	2.2	2.2	2.2
ε_t	0.00008	0.00008	0.00008	0.00008	0.00008	0.00008	0.00008

As presented in Table 4.2 above, loading conditions varied depending on the angle which applied the principal strains on the panel elements.

Table 4.3. Reinforcement alignment angles relative to the applied principal stress for different panel series tested by Mansour and Hsu (2005).

Panel Series:	**CA-series & CB-series**	**CD-series**	**CE-series**
Reinforcement Angle (α_2) vs. Applied Stress	$\alpha_2 = 45^o$	$\alpha_2 = 68.2^o$	$\alpha_2 = 90^o$

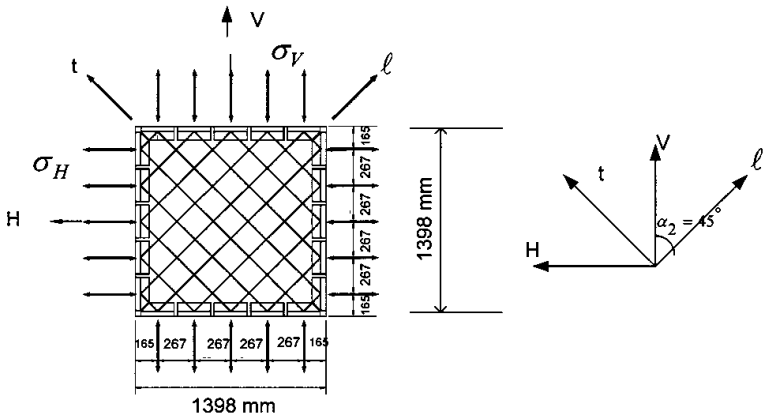

(d) Steel bar orientation in panels of CA-series and CB-series ($\alpha_2 = 45^\circ$)

Figure 4.2. Steel bar orientation in panels of CA-series and CB-series ($\alpha_2 = 45^o$) (Mansour and Hsu 2005).

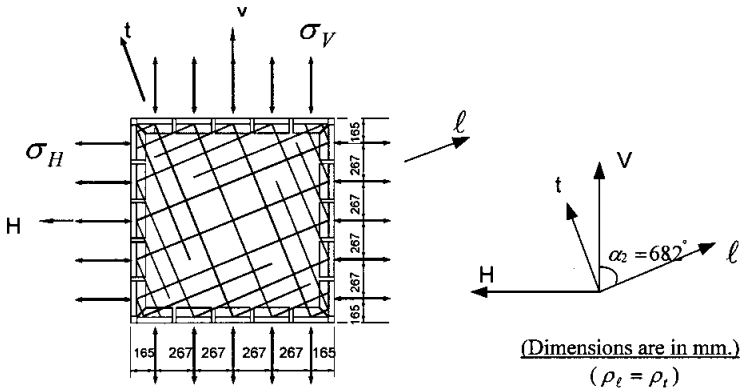

(c) Steel bar orientation in panels of CD-series (α_2 = 68.2°)

Figure 4.3. Steel bar orientation in panels of CD-series ($\alpha_2 = 90^o$) (Mansour and Hsu 2005).

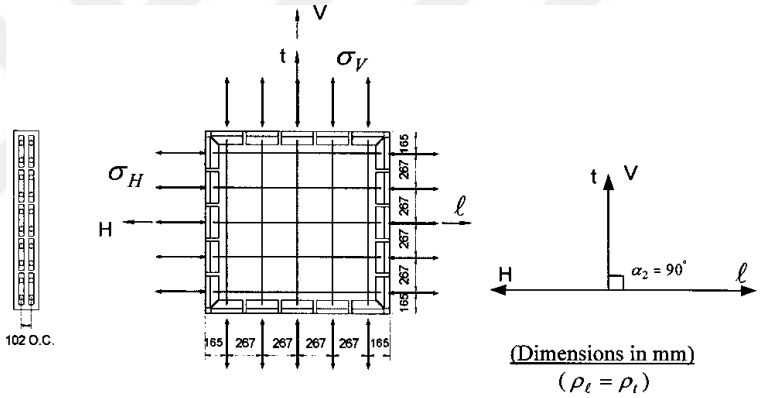

(a) Steel bar orientation in panels of CE-series (α_2 = 90°)

Figure 4.4. Steel bar orientation in panels of CE-series ($\alpha_2 = 68.2^o$) (Mansour and Hsu 2005).

4.3. Parametric Sensitivity Analyses on Selected Specimens

In this study, a set of comprehensive parametric sensitivity analysis were carried out on selected specimens (SE8 and SE10 from Stevens, 1987; CB3, CB4 and CD4 from Mansour and Hsu, 2005). These specimens were selected from 15 different panel tests (12 from Mansour and Hsu, 2005; and 3 from Stevens, 1987) since these five (5) specimens were susceptible to the friction coefficient defined in the model, which was identified as the only variable impacting model results. Since panel series were

constructed in consideration of different parameters (e.g., different reinforcement configurations and loading conditions), it is reasonable to study the sensitivity of these panel specimens to the friction coefficient that was defined in the model.

Ranges of friction coefficients that can capture the overall behavior of each selected specimen were defined. Analyses were conducted using these pre-defined set of friction coefficients, ranging from 0 to 0.25, with increasing increments of 0.05. Model predictions with these friction coefficients in the range of 0:0.05:0.25 are presented in Figure 4.5 to Figure 4.9. All model estimations were compared with test results provided by Stevens (1987) or Mansour and Hsu (2005). A summary of the parametric sensitivity studies carried out and optimum friction coefficients identified for each of the specimen are available in Table 4.4. As presented in Table 4.4, it was seen that only five specimens (SE8, SE10, CB3, CB4 and CD4) were sensitive to the coefficient of friction defined in the model. In that sense, these five specimens were tested for different friction coefficients and the results are discussed in the following sections.

Table 4.4. Parametric Sensitivity Matrix summarizing sensitivity programme and optimal results.

S[1]/FC[2]	**SE8**	**SE9**	**SE10**	**CA2**	**CA3**	**CA4**	**CB3**	**CB4**	**CD4**	**CE4**
Series	Stevens (1987)			Mansour and Hsu (2005)						
0.00	-[3]	0[3]	-	0	0	0	-	-	+	0
0.05	+	0	-	0	0	0	-	-	-	0
0.10	-	+	-	0	0	0	-	-	-	0
0.15	-	0	+	0	0	0	-	+	-	0
0.20	-	0	-	+	+	+	+	-	-	+
0.25	-	0	-	0	0	0	-	-	-	0

4.3.1. Sensitivity Studies for Specimens Tested by Stevens (1987)

Parametric sensitivity results provided by the improved FSAM conducted for specimen SE8 (Stevens 1987) using a pre-defined set of friction coefficients (in the

range of 0:0.05:0.25) are presented in Figure 4.5 . As a result of the analyses carried out using different friction coefficients, it was observed that the optimal friction coefficient for specimen SE8 is equal to 0.05. Model predictions at global and local response levels using this friction coefficient (η=0.05) are presented in Section 4.4. At first glance, it seems that using a zero-friction coefficient (η=0.00) yields better results for the shear stress capacity in the positive load direction; however, wwhen the model results are carefully investigated, it is seen that Figure 4.5a shows that using zero-friction coefficient underestimates the negative shear capacity and fails to capture the cyclic behavior pattern of the experimental results whereas a friction coefficient of 0.05 better captures the cyclic behavior pattern with minor capacity overestimations in higher cycles.

Figure 4.6 presents the parametric sensitivity results for specimen SE10 (Stevens 1987) using the same set of friction coefficients with specimen SE8 (in the range of 0:0.05:0.25). Comparisons of model and test results presented in Figure 4.6 reveals that friction coefficients in the range of 0 to 0.05 do not yield optimal results. Selecting the optimal friction coefficient for this specimen is not as straightforward as other specimens investigated. Although selecting higher friction coefficients (e.g. coefficients larger than 0.20 or 0.25) seems to capture the shear stress capacity, degradation in the last cycle was not well-simulated using these parameters. Therefore, 0.15 was selected as the optimal friction coefficient despite the minor underestimation of the shear capacity compared to Figure 4.6e and Figure 4.6f.

Specimen SE9, which is symmetrically reinforced and subjected to a pure shear stress state, model results are not sensitive to the value of the friction coefficient, since shear strains do not develop along the cracks. In the case of Specimen SE10, although it is non-symmetrically reinforced (similar to SE8), the normal stresses applied on the specimen reduce the impact of the friction coefficient on the model response,

[1]S: Specimen.

[2]FC : Friction Coefficient (η).

[3](-) sign means an analysis was made with the corresponding coefficient but results were not optimum.

[4](0) means friction coefficient doesn't impact the model results.

best fit for the shear stress-strain response is obtained when the friction coefficient is defined as 0.15 and for specimen SE8 it is 0.05. Average of the all optimal aggregate interlock friction coefficient values for the specimens tested by Stevens (1987) is equal to 0.10. Same friction coefficient was also used in the study conducted by Orakcal *et al.*, (2012), where in the underlying model of that study dowel action and cyclic degradation parameters were neglected. It was observed that average of the optimal friction coefficient for these three specimens did not change significantly, implying that accounting dowel action with cyclic degradation parameters balanced each other to some extent and resulting in the same friction coefficient of 0.10 for this panel series.

4.3.2. Sensitivity Studies for Specimens Tested by Mansour *et al.*, (2005)

Parametric sensitivity studies for the coefficient of friction (in the range of 0:0.05:0.25) for specimens CB3, CB4 and CD4 presented in Figure 4.7 to Figure 4.9, respectively. As shown in Figure 4.7, using a friction coefficient smaller than 0.20 resulted in an underestimation of the shear capacity. Although this discrepancy decreased when a friction coefficient close to 0.20 was used, whereas model predictions did not change significantly when a friction coefficient larger than 0.20 was used. Based on these observations, the optimal friction coefficient was selected as 0.20 for specimen CB3.

Sensitivity analyses carried out using relatively high (0.20 and 0.25) and low (zero to 0.05) friction coefficients indicate that moderate (relatively) coefficients provides better simulation for specimen CB4. Using higher coefficients result in overestimation of the shear capacity in all cycles, whereas using lower coefficients fail to capture the shear capacity by underestimating it in initial cycles and overestimating it in later cycles, as well as the degradation in higher strain levels are not simulated by low friction coefficients. Although friction coefficients used in the parametric studies do not dominate model predictions, friction coefficient of 0.15 was selected as the optimal friction coefficient as it allows the model to capture the shear stress degradation of this specimen. Figure 4.9 demonstrates that as the friction coefficient increases, shear stress degradation in model predictions for higher cycles disappear, except that in the first two cycles, the shear stress capacities do not change significantly. Model results suggest

that using a friction coefficient of 0.00, which represents zero aggregate interlock due to the frictional resistance, yields the best results in capturing the overall response of specimen CD4. Since model incorporates other shear transfer mechanisms across cracks (i.e. dowel action as suggested by He and Kwan (2001) with cyclic degradation parameters applied as explained in the Chapter 3), having zero friction coefficient is reasonable as the dowel action with the cyclic degradation parameters still capture the overall behavior without consideration of elasto-plastic friction (as proposed by Orakcal, 2012). Therefore, for this specimen a friction coefficient of 0.00 was selected and the global and local response predictions of the model are presented in Section 4.4.

For specimen CA2, CA3, CA4, and CE4, model results are not sensitive to the friction coefficient, due to the loading conditions imposed on these specimens and symmetry of the reinforcement. Differences in model results are observed for Specimens CB3, CB4, and CD4. All model results presented for the test specimens by Mansour (2005) are generated using a friction coefficient in the range of 0.15 to 0.20 (except CD4). Similar to the tests by Stevens (1987), modification of the friction coefficient noticeably changes the analytical response obtained for some of these specimens. A friction coefficient of 0.20 was also used in the study by Orakcal *et al.*, (2012), however in this study dowel action and clamping effects as well as the cyclic degradation parameters were neglected. Similar to the specimens tested by Stevens (1987), optimal friction coefficients for specimens tested by Mansour (2005) did not alter significantly due to the implementation of dowel action with cyclic degradation parameters.

In conclusion, sensitivity studies provided optimal friction coefficients for each specimen susceptible to the friction coefficient as presented in Table 4.5. Based on the results and observations, an optimal range of friction coefficient was identified for each panel series separately: 0.10 for SE-series and 0.15-0.20 for C-series (except CD4). Similar to the discrepancy in tension stiffening behavior observed in these two experimental programs (Bentz, 2005), the necessity of using different interlock friction coefficients to obtain the best correlation between model and test results for the two programs can be attributed to different shear aggregate interlock characteristics of the specimens, such as maximum aggregate size of concrete and spacing of reinforcing steel

bars.

Table 4.5. Optimal friction coefficients for each specimen susceptible to the friction coefficient.

	SE8	**SE10**	**CB3**	**CB4**	**CD4**
η	0.05	0.15	0.20	0.15	0.00

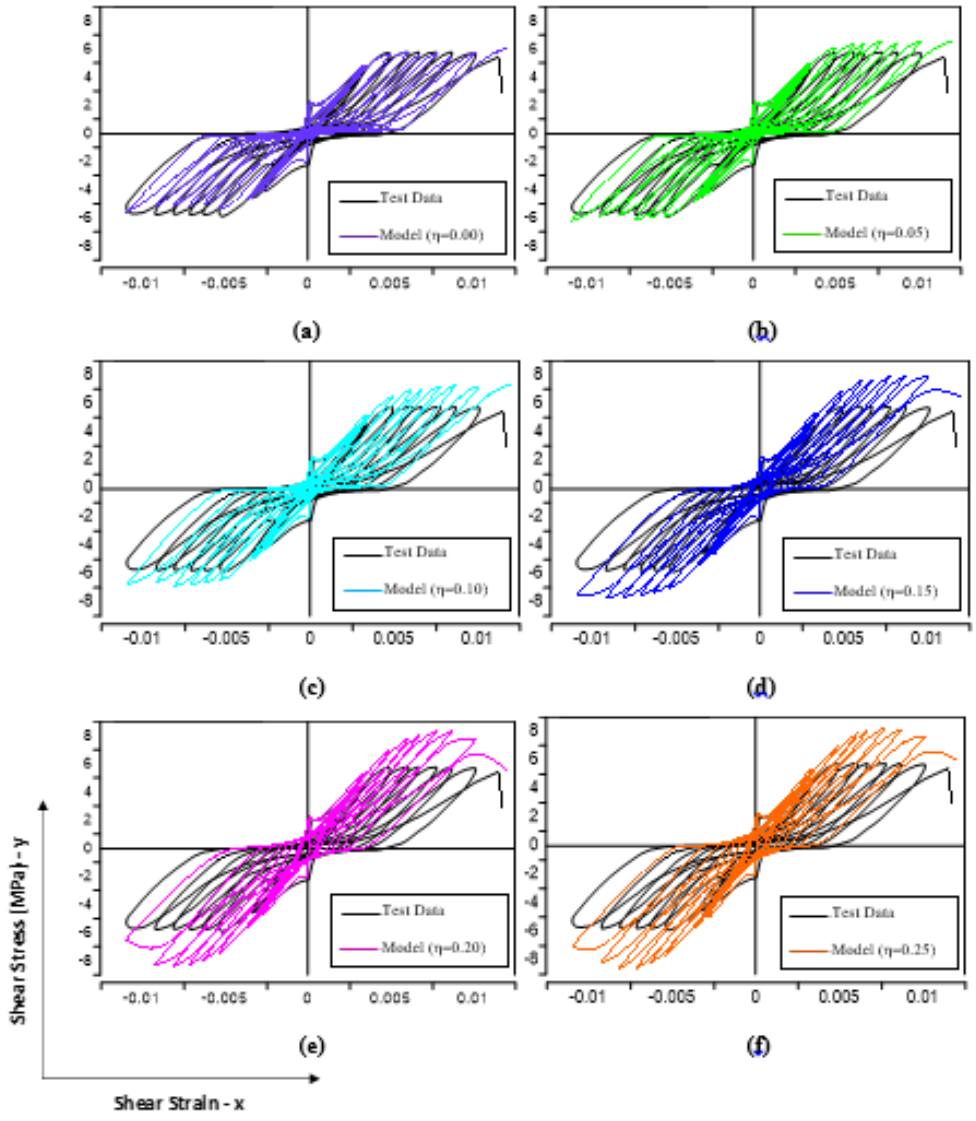

Figure 4.5. SE8 : Shear stress (MPA) vs. Shear Strain (y-x) graphs for different friction coefficients compared with test data presented in the order of (a) η=0.00, (b) η=0.05, (c) η=0.10, (d) η=0.15, (e) η=0.20, (f) η=0.25.

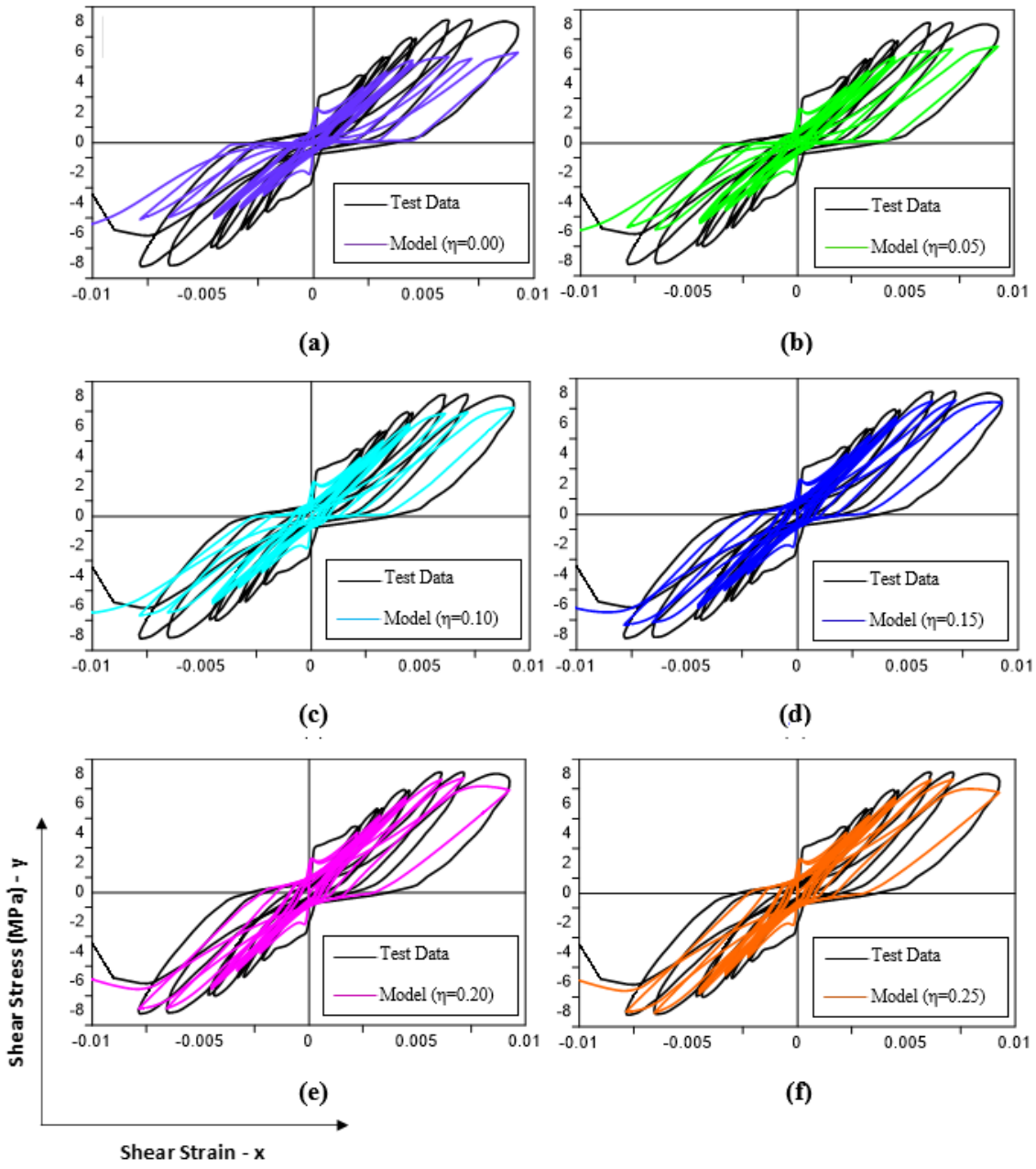

Figure 4.6. SE10 : Shear stress (MPA) vs. Shear Strain (y-x) graphs for different friction coefficients compared with original test data presented in the order of (a) η=0.00, (b) η=0.05, (c) η=0.10, (d) η=0.15, (e) η=0.20, (f) η=0.25.

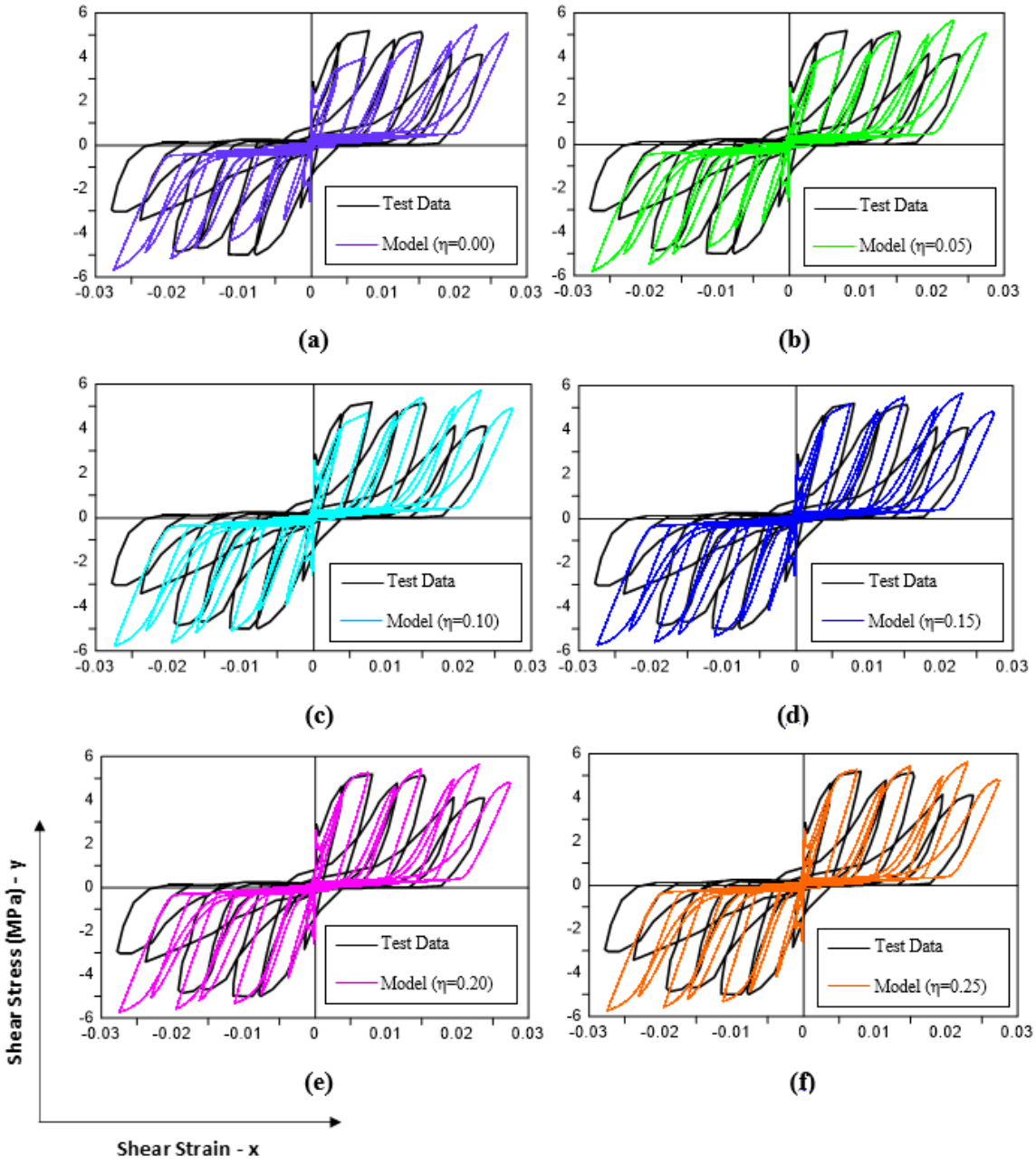

Figure 4.7. CB3: Shear stress (MPA) vs. Shear Strain (y-x) graphs for different friction coefficients compared with original test data presented in the order of (a) η=0.00, (b) η=0.05, (c) η=0.10, (d) η=0.15, (e) η=0.20, (f) η=0.25.

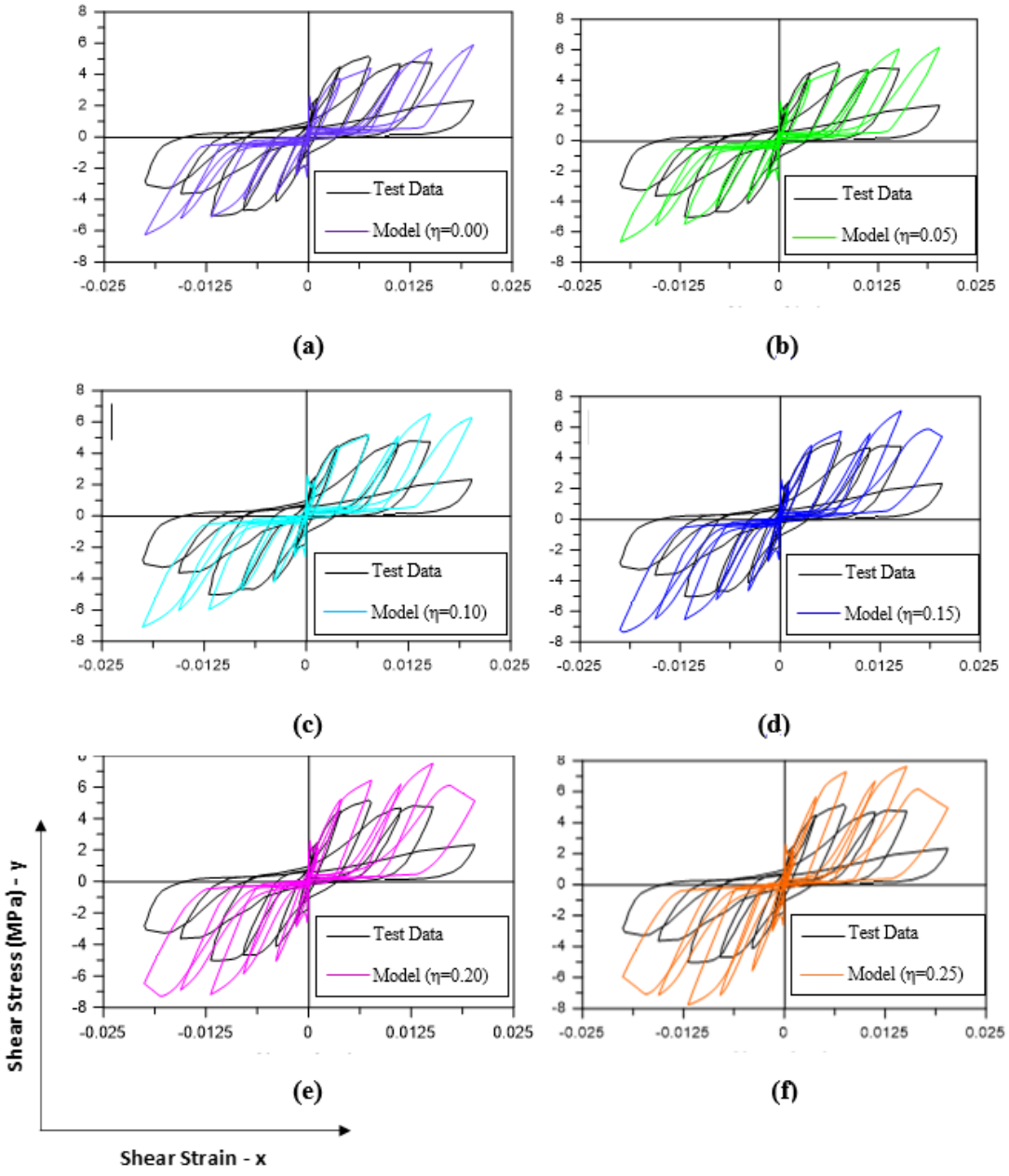

Figure 4.8. CB4: Shear stress (MPA) vs. Shear Strain (y-x) graphs for different friction coefficients compared with original test data presented in the order of (a) η=0.00, (b) η=0.05, (c) η=0.10, (d) η=0.15, (e) η=0.20, (f) η=0.25.

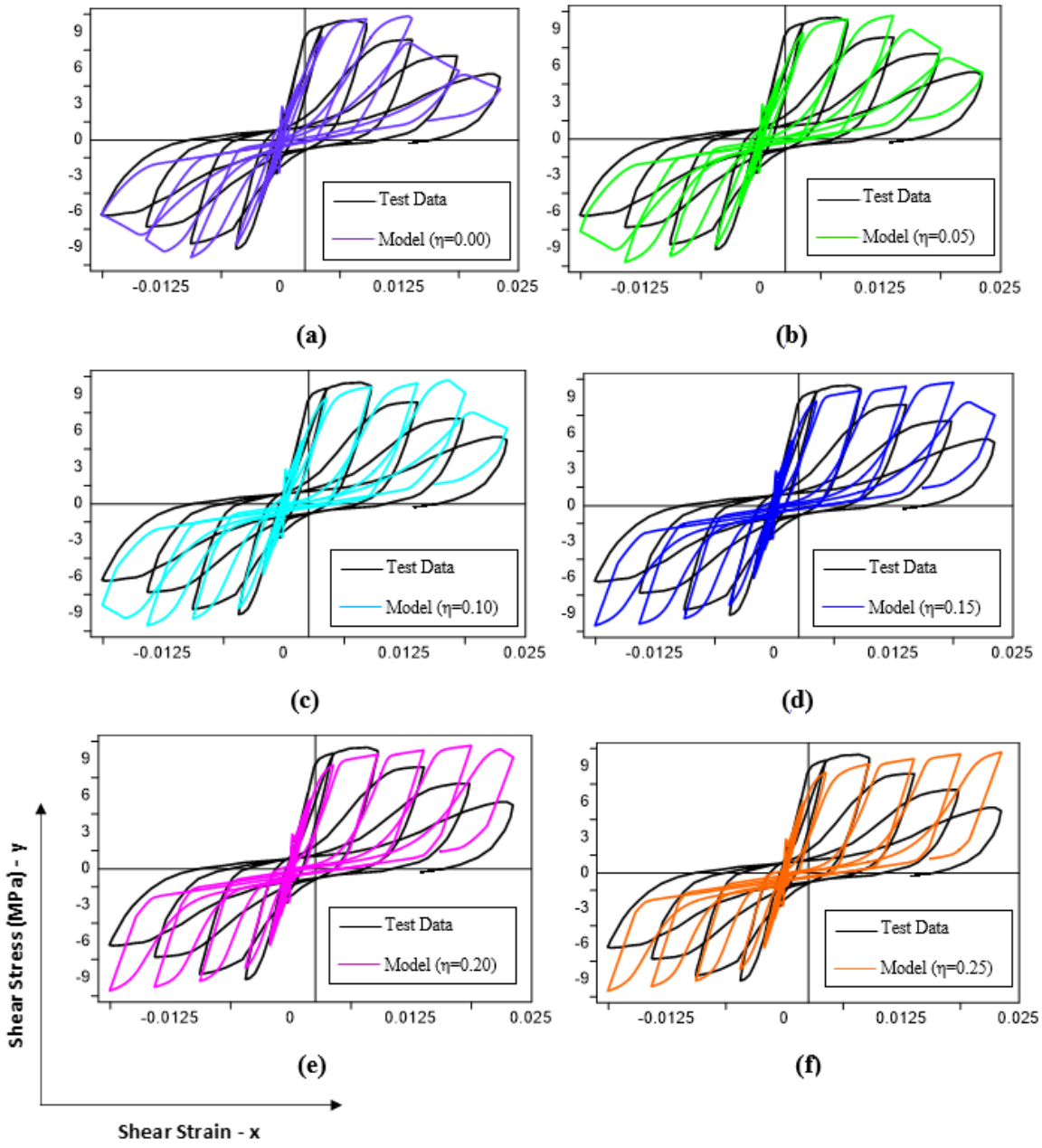

Figure 4.9. CD4: Shear stress (MPA) vs. Shear Strain (y-x) graphs for different friction coefficients compared with original test data presented in the order of (a) η=0.00, (b) η=0.05, (c) η=0.10, (d) η=0.15, (e) η=0.20, (f) η=0.25.

4.4. Model Predictions vs. Panel Test Results by Stevens (1987)

In this section, global and local response predictions of the model for specimens SE8, SE9 and SE10 are presented using their optimum friction coefficients.

4.4.1. Global Response of SE8

As shown in Figure 4.10, overall shear stress vs. shear strain response of specimen SE8 is estimated by the improved model accurately. Since this specimen had asymmetrical reinforcement along x and y directions, the model was calibrated to determine an optimal friction coefficient as explained in Section 4.3.1. It is observed that the red line drawn by the model follows the path of the test data both during loading and unloading curves, resulting in nearly overlapping results between model and test results. The shear stress capacity was also captured in an acceptable range although it is slightly overestimated (less than 10% difference compared to test data). Model prediction is also in line with the stiffness characteristics of the specimen. Moreover, pinching effect (which is generally associated with shear behavior) and cracking shear stress level are also well captured by the model. Since Specimen SE8 had 1% reinforcement ratio in the y direction and 3% in the x direction (see Table 4.1), while the reinforcement in y direction yielded, the reinforcement in x direction remained linear elastic. Yielding of reinforcement in y direction not only limited the capacity, but also generated a ductile behavior for the specimen.

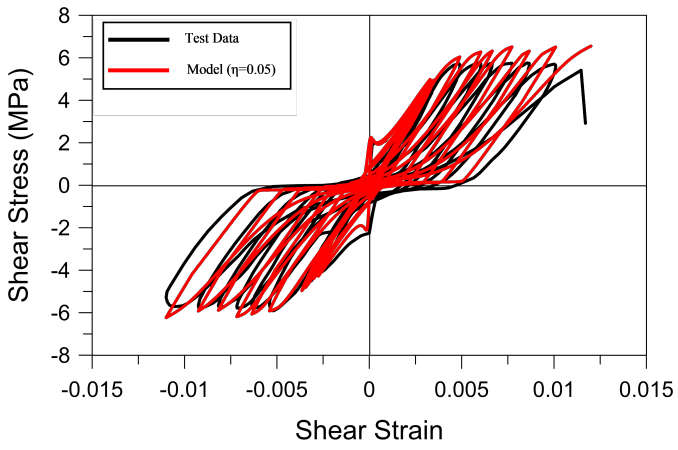

Figure 4.10. SE8: Comparison of Shear Stress vs. Strain graphs of Test Data and Model using a friction coefficient of 0.05.

For visualizing the results of the improved model compared to the results of the original FSAM, a comparison graph is presented below. In the below figure, it is clearly

observed that the model developed under the scope of this study provides improved results compared to the original FSAM.

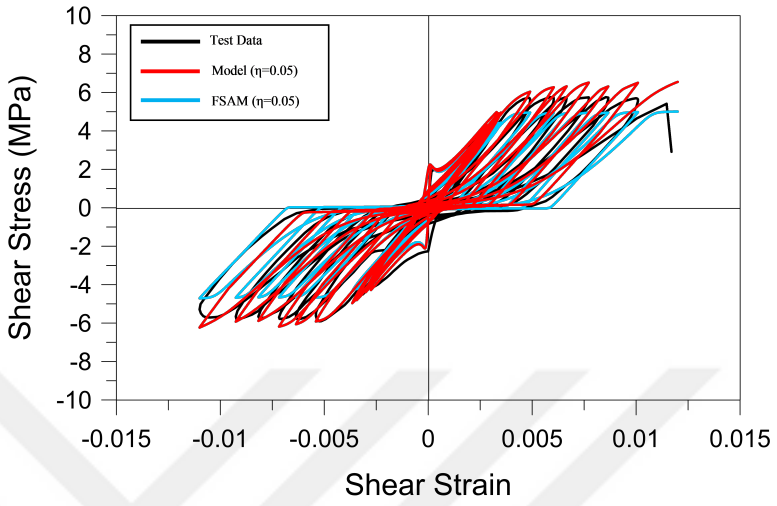

Figure 4.11. SE8: Comparison of Shear Stress vs. Strain graphs of Test Data vs. Model and original FSAM using a friction coefficient of 0.05.

General behavior of Specimen SE9 is captured by the model with reasonable accuracy (Figure 4.12). It is important to note that, unlike other specimens in test specimens provided by Stevens (1987), specimen SE9 was not susceptible to the friction coefficient defined in the model due to its symmetrical reinforcement configuration and loading condition (which was pure shear). Therefore, the average of friction coefficients used for specimens SE8 (0.05) and SE10 (0.15) was defined as the friction coefficient (0.10) of this specimen during the analysis. Although the shear stress capacity appears to be slightly overestimated by the model (by 11% of the test measurement); pinching characteristics, cracking stresses, and cyclic stiffness properties of the behavior are all well-predicted (Figure 4.12).The widths of the loading and unloading loops in the stress-strain behavior are predicted to be only slightly narrower than the test results, with the cumulative area under the loops estimated at 88% of the experimentally-measured response. The main reason of this discrepancy may be attributed to variation in the cyclic behavior of concrete, which governs the overall response of this specimen. As a measure of ductility, the shear strain capacity of the specimen (at which degradation in shear stress initiates), is well-estimated by the model, at approximately 95% of the test

result. Since the specimen has 3% reinforcement in both directions, in the model for this specimen, the concrete compression struts are able to reach their maximum "softened and damaged" compressive stress capacity, prior to yielding of steel. However, since the tests were stress-controlled, none of these tests were continued until the failure mode of the specimens was clearly identified.

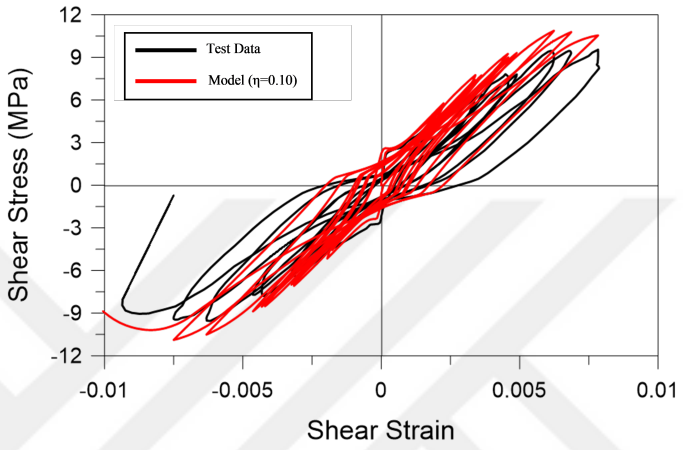

Figure 4.12. SE9: Comparison of Shear Stress vs. Strain graphs of Test Data and Model using a friction coefficient of 0.10.

4.4.2. Global Response of SE10

Physically identical to SE8 (e.g., asymmetrical reinforcement ratios in both directions and thickness etc.), specimen SE10 had another controlling variable different from SE8, which was the applied compressive normal stresses (σ_x and σ_y) during testing. This specimen was unique due to its reinforcement configuration and loading condition. Due to its asymmetrical reinforcement configuration, the FSAM was calibrated with the optimal friction coefficient of 0.15 similar to SE8. Although shear stress capacity is slightly underestimated, it is observed that overall behavior (e.g. cracking stress, stiffness of the loading and unloading curves and pinching features) is well-predicted.

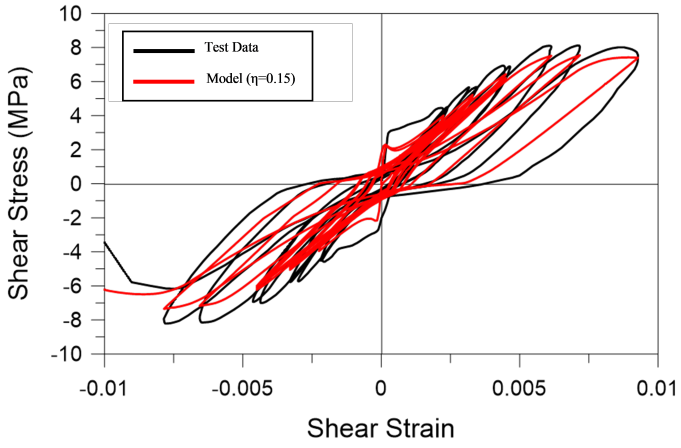

Figure 4.13. SE10: Comparison of Shear Stress vs. Strain graphs of Test Data and Model using a friction coefficient of 0.15.

4.4.3. Local Responses of SE8

Local response predictions of the improved model for specimen SE8, including normal strains in x and y directions, principal strain directions and principal stress directions are compared with test results in this section. As illustrated in Figure 4.14 and Figure 4.15, normal strain history in both directions (x and y) are accurately predicted by the model within an acceptable margin. Response predictions at critical data points (e.g. sudden changes in recorded normal strain values) were also accurately simulated by the model. Additionally, as shown in Figure 4.15, despite the existence of fluctuations during loading, experimentally observed principal strain history for specimen SE8 is also reasonably presented. When the principal stress direction in concrete versus panel shear stress behaviors are compared for Specimen SE8 (Figure 4.17), it is observed that the model predictions for the principal stress direction in concrete do not noticeably deviate from the two crack directions. Discrepancies between the model predictions and test results may be attributed to the simplicity of the implemented shear transfer mechanisms across cracks although it shows more complicated behavior during the experiment as well as the reversals during loading/unloading of the specimen. As mentioned above, predicted principal strain directions rotate with the measured ones whereas predicted principal stress directions do not deviate with the

measured ones. As expected, due to underlying assumption (fixed crack angles after formation of cracks) and mechanism of FSAM (Ulugtekin 2010), the predictions of the model successfully captured this behavior.

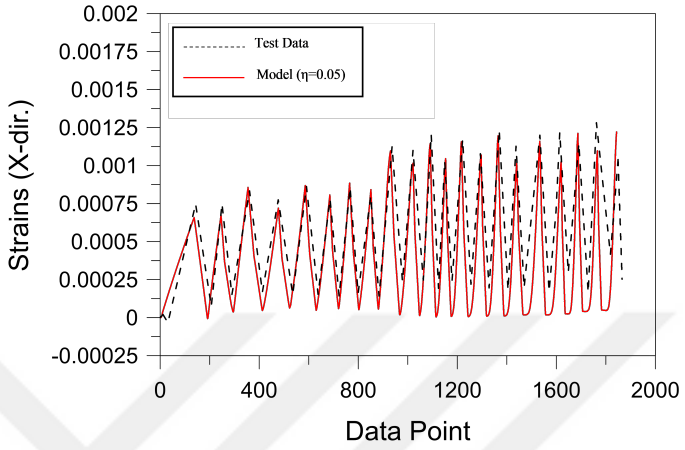

Figure 4.14. SE8: Comparison of Strains in X-direction of Test Data and Model using a friction coefficient of 0.05.

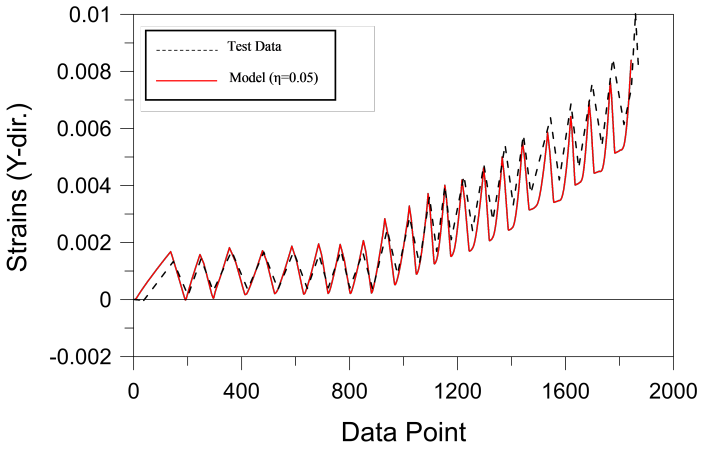

Figure 4.15. SE8: Comparison of Strains in Y-direction of Test Data and Model using a friction coefficient of 0.05.

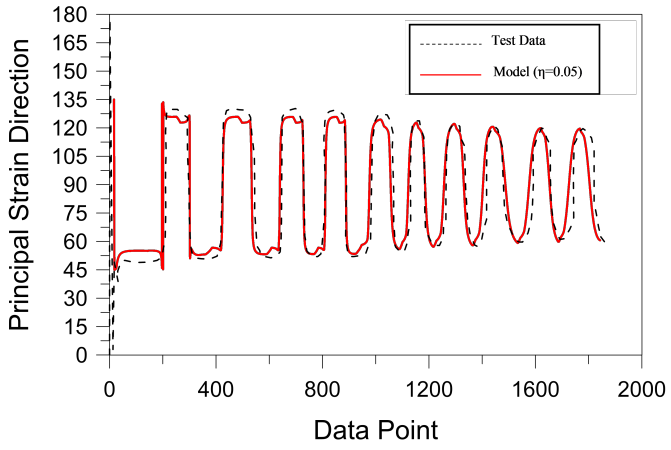

Figure 4.16. SE8: Comparison of Principal Strain Directions of Test Data and Model using a friction coefficient of 0.05.

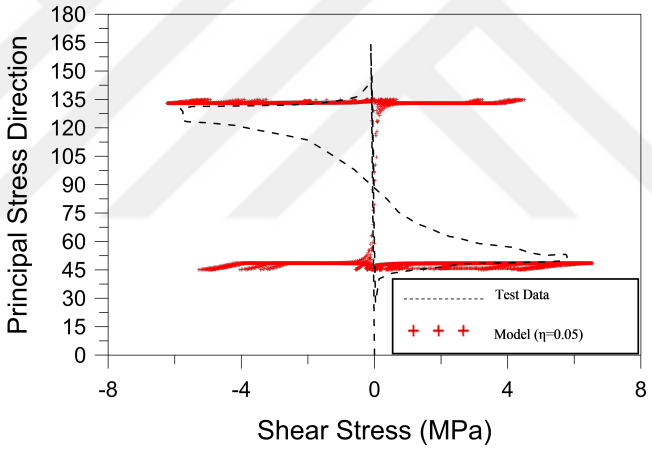

Figure 4.17. SE8: Comparison of Principal Stress Directions of Test Data and Model using a friction coefficient of 0.05.

4.5. Local Responses of SE9

For specimen SE9, normal strain history in x-direction is well-predicted (Figure 4.18) whereas at later stages of loading the predicted normal strains in y-direction deviates from the measured strain history (Figure 4.19). As presented in Section 4.1, this specimen had symmetrical reinforcement and was subjected to pure shear stress condition. Considering the identical reinforcement configuration in both orthogonal directions for this specimen and observing that the predicted strain history in both

orthogonal directions are nearly identical (red lines in Figure 4.18 and Figure 4.19), deviations between test results and model predictions can be explained by the imperfections during the experiments. When the principal strain directions are compared for this specimen, as depicted in Figure 4.20, test results are well-predicted by the model. Model predictions for the principal strain directions are 45o and 135o, since the pure shear stress state applied on the symmetrically reinforced specimen creates a pure shear strain state, which is also observed in the test measurements. Also due to the pure shear stress state applied on the symmetrically reinforced specimen, the principal stress directions in concrete predicted by the model are naturally 45o and 135o during the entire loading history, which is also in agreement with the test results, as shown in Figure 4.21.

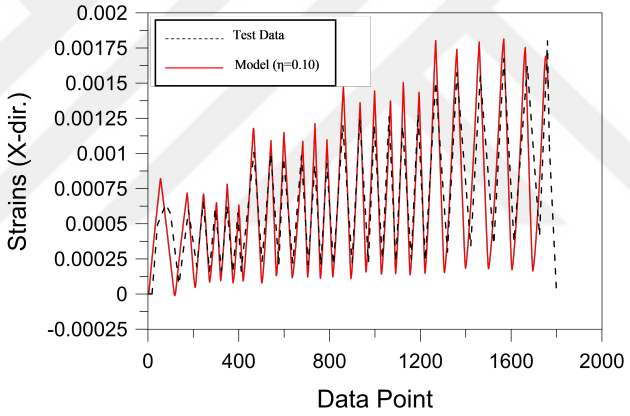

Figure 4.18. SE9: Comparison of Strains in X-direction of Test Data and Model using a friction coefficient of 0.10.

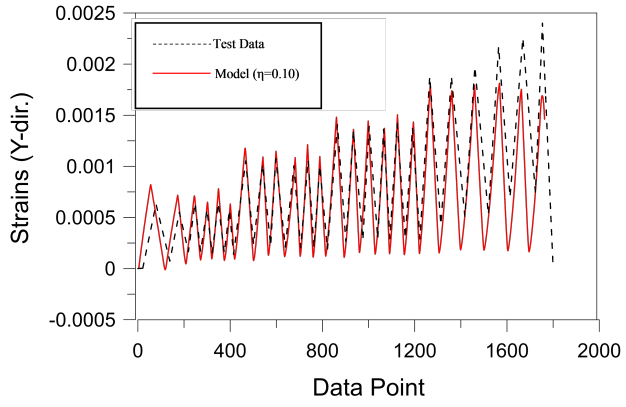

Figure 4.19. SE9: Comparison of Strains in Y-direction of Test Data and Model using a friction coefficient of 0.10.

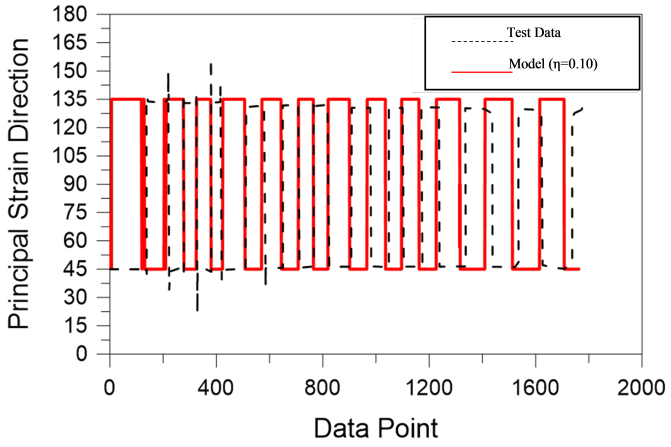

Figure 4.20. SE9: Comparison of Principal Strain Directions of Test Data and Model using a friction coefficient of 0.10.

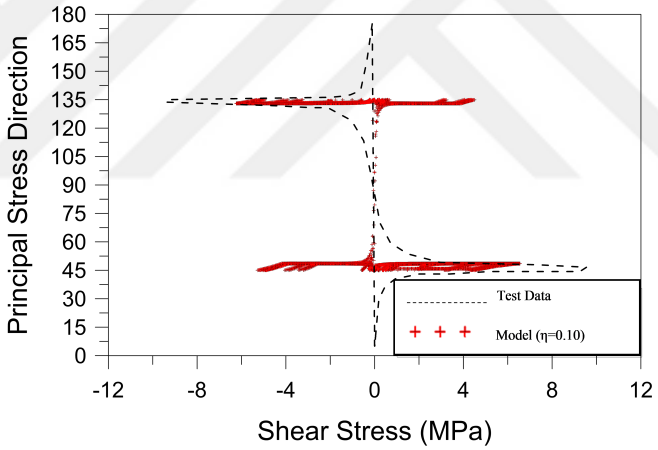

Figure 4.21. SE9: Comparison of Principal Stress Directions of Test Data and Model using a friction coefficient of 0.10.

4.5.1. Local Responses of SE10

For specimen SE10, it is observed that the normal strain history in y-direction is well-predicted (Figure 4.23) by the improved FSAM whereas normal strain history predictions in x-direction is relatively high compared to the measured strains. Nonetheless, the overall trend is accurately captured in x-direction (Figure 4.22). When the principal strain directions are compared, as shown in Figure 4.23, the test measure-

ments are predicted accurately by the model. The measured and predicted principal stress directions in concrete (vs. shear stress on the panel) are compared in Figure 4.25. Similarly to Specimen SE8, although there is experimentally-observed variation in the direction of the principal concrete stresses with shear stress, as shown in Figure 4.25, such variation is typically within the unloading and reloading branches of the response, the upper and lower bounds of the measured principal stress directions do not vary significantly with the magnitude of the shear stress, and are in good agreement with model predictions, validating the modeling approach used.

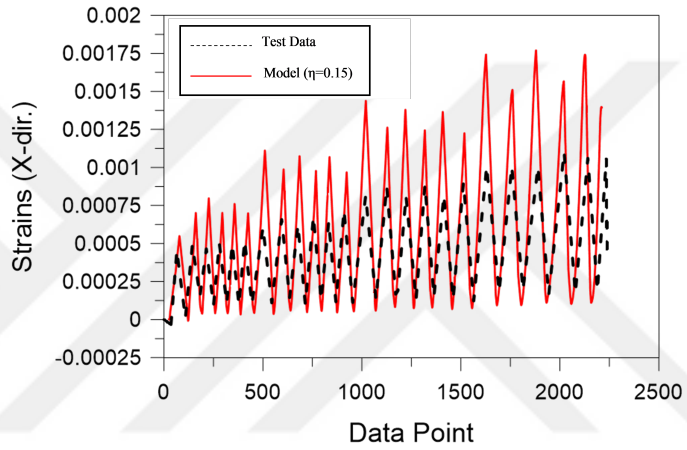

Figure 4.22. SE10: Comparison of Strains in X-direction of Test Data and Model using a friction coefficient of 0.15.

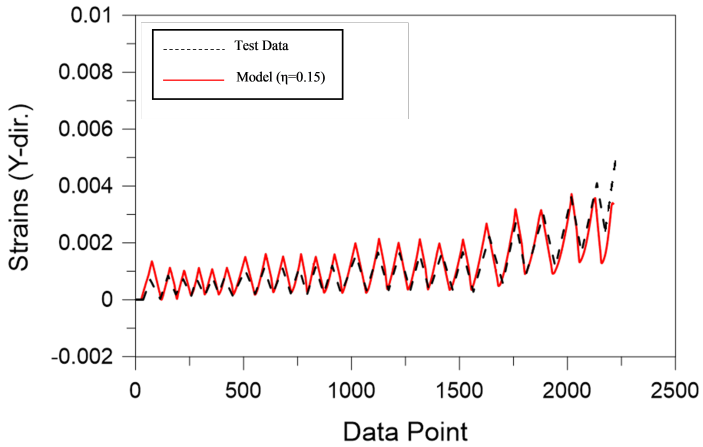

Figure 4.23. SE10: Comparison of Strains in Y-direction of Test Data and Model using a friction coefficient of 0.15.

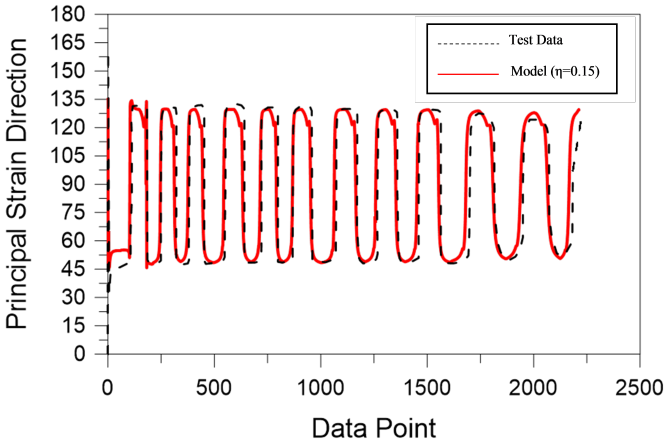

Figure 4.24. SE10: Comparison of Principal Strain Directions of Test Data and Model using a friction coefficient of 0.15.

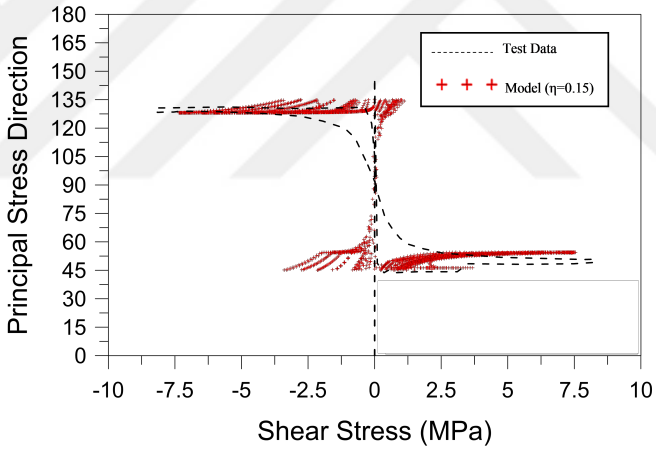

Figure 4.25. SE10: Comparison of Principal Stress Directions of Test Data and Model using a friction coefficient of 0.15.

4.6. Model Predictions vs. Panel Test Results by Mansour and Hsu (2005)

In this section, comparison of global and local response predictions with test results for specimens CA2, CA3, CA4, CB3, CB4, CD4 and CE4 are presented using their optimum friction coefficients.

4.6.1. Global Response of CA2

As presented in Figure 4.26, model is capable of predicting the shear stress capacity of this specimen with only minor overestimations in the last cycles. Other features of the response including the shapes of the unloading and reloading curves, stiffness characteristics, cracking stress values, and pinching behavior (to some extent) are captured with reasonable accuracy. As illustrated in Table 4.2, the specimen CA2 has the lowest reinforcement ratio in both directions with a value of 0.0077. Since the specimen has relatively low amount of reinforcement in both directions, the behavior is dominated by yielding of reinforcing steel in both test results and model predictions.

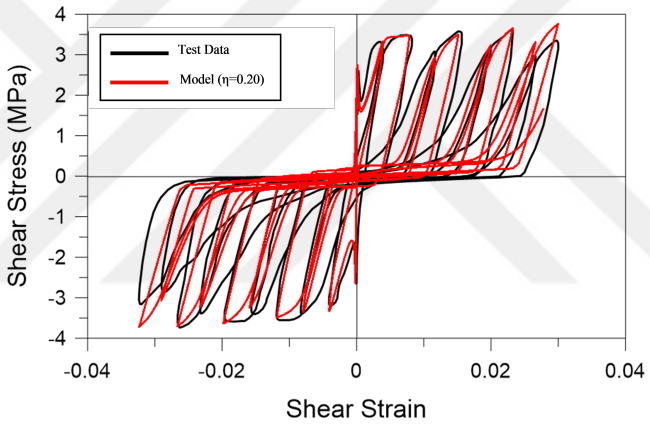

Figure 4.26. CA2: Comparison of Shear Stress vs. Strain graphs of Test Data and Model using a friction coefficient of 0.20.

For visualizing the results of the improved model compared to the results of the original FSAM, a comparison graph is presented below. In the below figure, it is clearly observed that the model developed under the scope of this study provides improved results compared to the original FSAM.

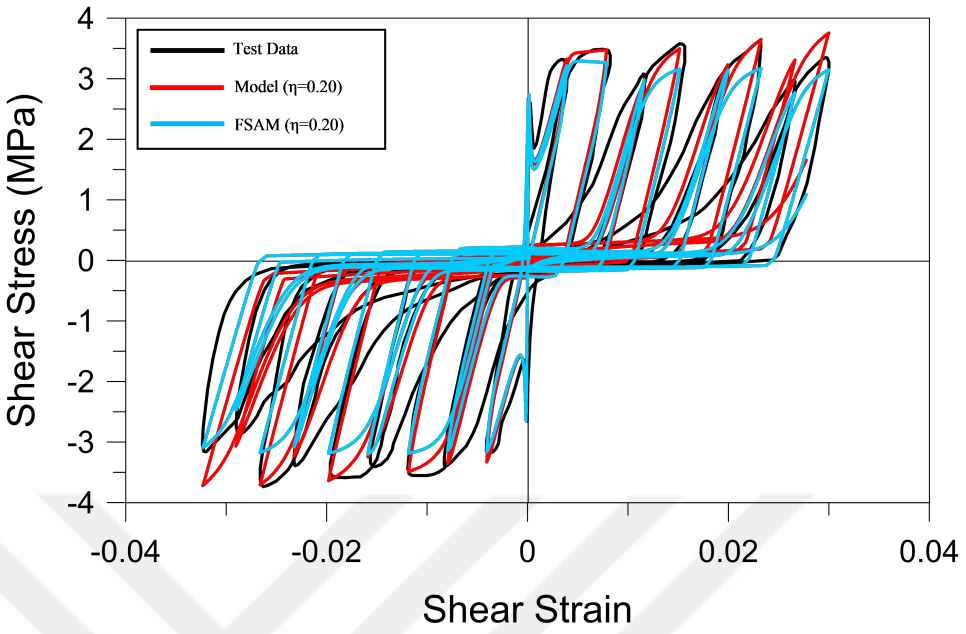

Figure 4.27. CA2: Comparison of Shear Stress vs. Strain graphs of Test Data versus Model and original FSAM using a friction coefficient of 0.20.

4.6.2. Global Response of CA3

The analytical model accurately predicts the overall shear stress vs. shear strain behavior of this specimen in terms of its stiffness, cracking stress, and pinching attributes (Figure 4.28). Initiation of the degradation in shear stress capacity and rate of degradation in shear stress capacity of the specimen are also well simulated by the model. The slight difference between model and test results is mostly associated with the shape of the envelope of the response, which was found to be influenced both by the shape of the concrete stress-strain behavior in compression and the effective yield strength of reinforcing steel. It should also be noted that this specimen had symmetrical reinforcement ratios in the x and y directions (see Table 4.2 above for details).

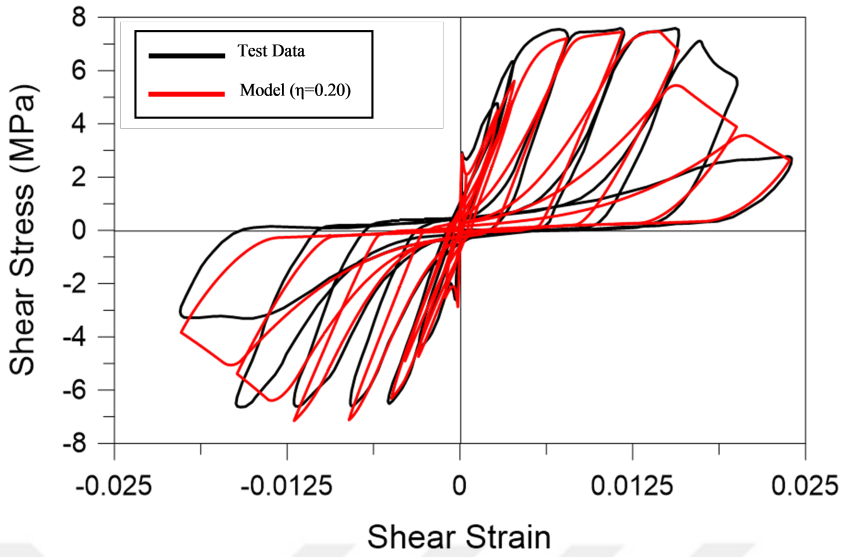

Figure 4.28. CA3: Comparison of Shear Stress vs. Strain graphs of Test Data and Model using a friction coefficient of 0.20.

4.6.3. Global Response of CA4

Specimen CA4 had the largest reinforcement ratio, with the value of 2.7% in both directions. The model well-predicts the overall shear stress vs. shear strain behavior of this specimen well, only with slight discrepancies in cyclic stiffness characteristics and rate of degradation in the last loading stages. Features including the pinching effect, cracking stress, and shear stress capacity are all captured accurately (Figure 4.29). The shear stress capacity of the specimen is captured with 100% accuracy, and similar to specimen CA3, model prediction for initiation of degradation in shear stress capacity is in good correlation with test results. The shape of the envelope of the predicted response was found to be significantly influenced by the shape of the concrete stress-strain behavior in compression.

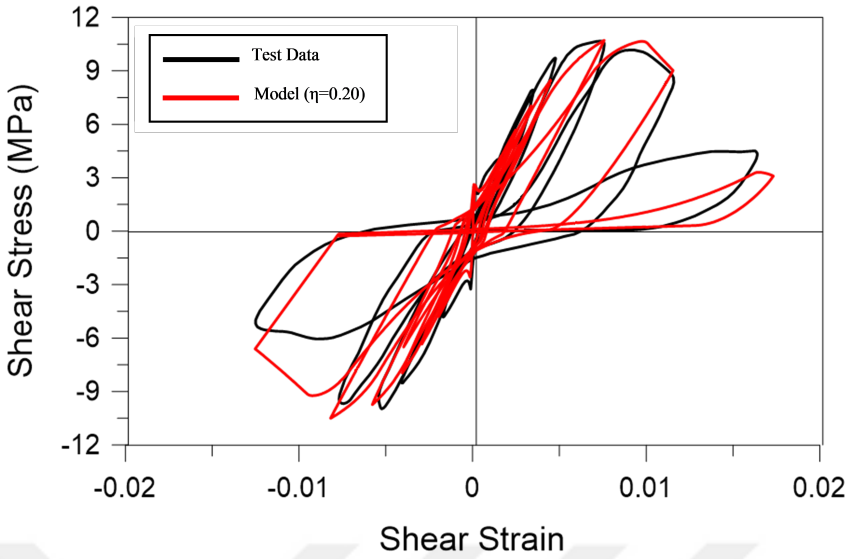

Figure 4.29. CA4: Comparison of Shear Stress vs. Strain graphs of Test Data and Model using a friction coefficient of 0.20.

4.6.4. Global Response of CB3

As explained and illustrated in Section 4.3, unlike CA-series, specimen CB3 is sensitive to the friction coefficient due to its reinforcement configuration (e.g., different reinforcement ratios in x and y directions). Therefore, for specimen CB3, 0.20 was defined as the optimal friction coefficient rather than using an arbitrary number. A similar approach was taken with the other specimens that were not sensitive to the friction coefficient. Compared to the predicted shape of the envelope of the response, shear stress capacity was predicted with less error (having high accuracy in initial cycles with some overestimation in later cycles). Specimen CB3 incorporated asymmetric reinforcement, and the overall response predicted by the model appears to be governed by yielding of reinforcement in y direction, having a lower reinforcement ratio (Figure 4.30) compared to its orthogonal direction. The hysteretic shape of the analytical response is considerably different than that of the experimentally-measured, as the test result shows a shape that seems to be influenced in-part by the concrete stress-strain behavior in compression. The model is capable of capturing the degradation in shear stress at high shear strains in positive loading direction.

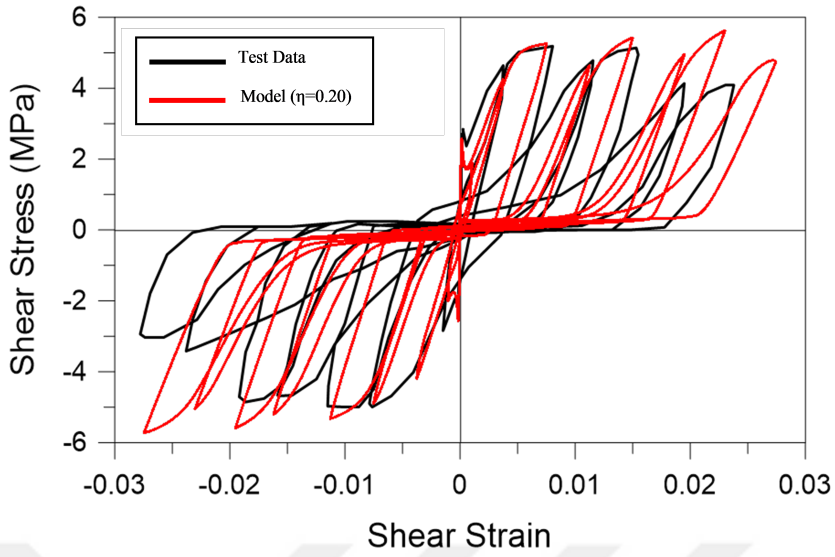

Figure 4.30. CB3: Comparison of Shear Stress vs. Strain graphs of Test Data and Model using a friction coefficient of 0.20.

4.6.5. Global Response of CB4

Specimen CB4 was similar to CB3, but with a larger reinforcement ratio in the x direction, which made the shape of the experimentally-measured response even more influenced by the concrete stress-strain behavior in compression (Figure 4.31). Shear stress capacity is captured at the initial cycles but at higher strains model overestimates test results, which may be attributed to the stress-strain envelope of concrete. Nonetheless, some degradation in shear stress capacity is observed in model prediction at the latest cycle in positive loading direction. As CB series are similar in terms of their construction properties, specimen CB4 was also found to be sensitive to the friction coefficient defined in the model similar to specimen CB3. As explained in Section 4.3, an optimal friction coefficient of 0.15 was applied during the analysis of specimen CB4.

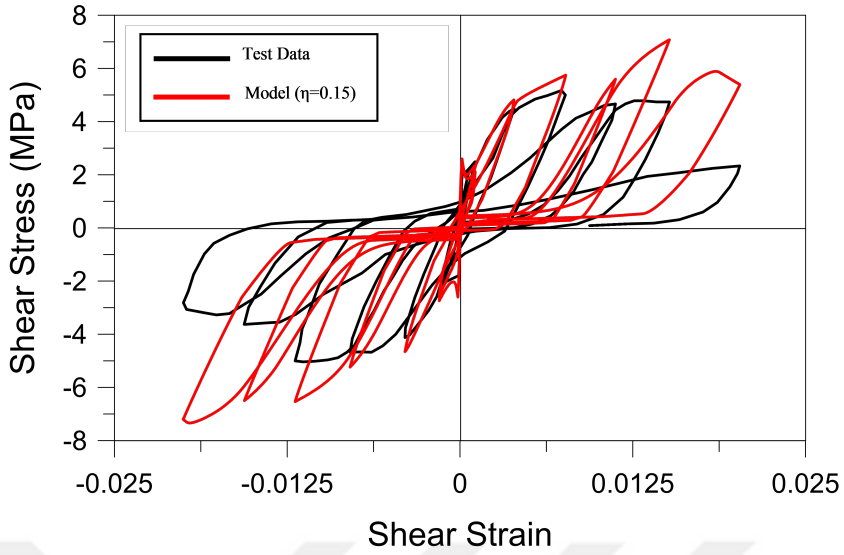

Figure 4.31. CB4: Comparison of Shear Stress vs. Strain graphs of Test Data and Model using a friction coefficient of 0.15.

4.6.6. Global Response of CD4

The model is capable of capturing the shear stress capacity and other behavioral features with reasonable accuracy (Figure 4.32). Model provides perfect matches for this specimen throughout the entire loading history including initiation of degradation in shear stress capacity and rate of degradation in shear stress. As explained in Section 4.3, construction parameters or loading conditions may impact the specimen's sensitivity to the shear friction coefficient. Specimen CD4 was subjected to a loading condition unlike any other specimen covered in Mansour and Hsu's experimental program, with applied normal and shear stresses on the specimen concurrently. For this specimen optimal friction coefficient was defined as zero (0), meaning that zero aggregate interlock is considered in model predictions. However, dowel action model implemented in the FSAM formulation with cyclic degradation parameter was employed in the model predictions for specimen CD4. Finally, a careful examination of Figure 4.32 implies that the response of concrete may have governed the behavior of this specimen.

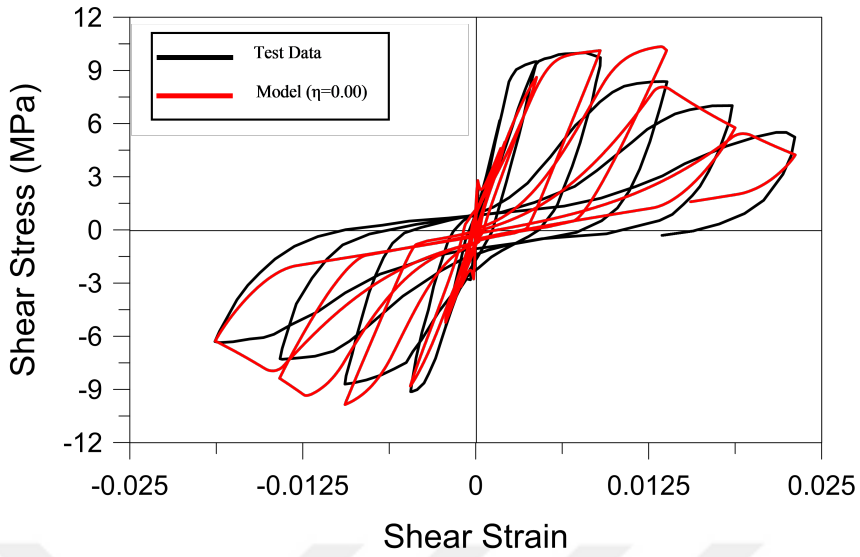

Figure 4.32. CD4: Comparison of Shear Stress vs. Strain graphs of Test Data and Model using a friction coefficient of 0.00.

4.6.7. Global Response of CE4

CE-series specimens were subjected to loading (normal stresses) parallel to the reinforcement directions. The model for specimen CE4 model recovers most features observed in the experimental response (stiffness, strength, hysteretic response), which is governed by the uniaxial stress vs. strain behavior of the reinforcing steel bars (Figure 4.33). The shear stress capacity predicted by the model for this specimen correspond to 100% of the experimentally-measured value, which validates the reliability of the uniaxial stress-strain model implemented in the FSAM for reinforcing steel.

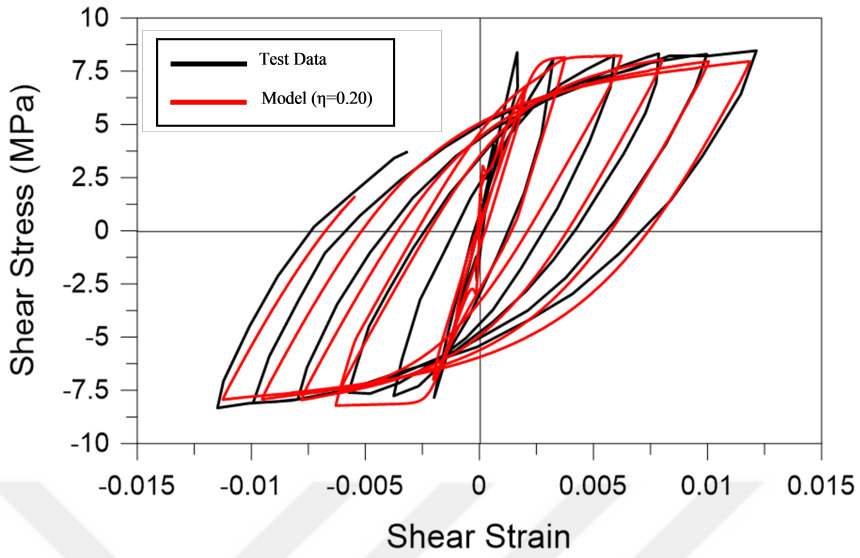

Figure 4.33. CE4: Comparison of Shear Stress vs. Strain graphs of Test Data and Model using a friction coefficient of 0.20.

4.6.8. Local Responses of CA Series Specimens

In this section, normal strains measured in x and y directions of representative test specimens are compared with model predictions. Since the reinforcement ratios were same in both directions for the CA-series specimens, it is expected that the normal strains in x and y directions should be approximately equal when the specimens are subjected to a state of pure shear stress. The model results consistently show this type of behavior, similar to the test results for the CA specimens, although some differences are observed during the last cycles (Figure 4.34 to Figure 4.37). When the model and test results are compared, the strain predictions in both x and y directions are reasonable for both specimens CA2 and CA3, but the residual (plastic) strains at the end of the test estimated by the model are consistently lower than the test results.

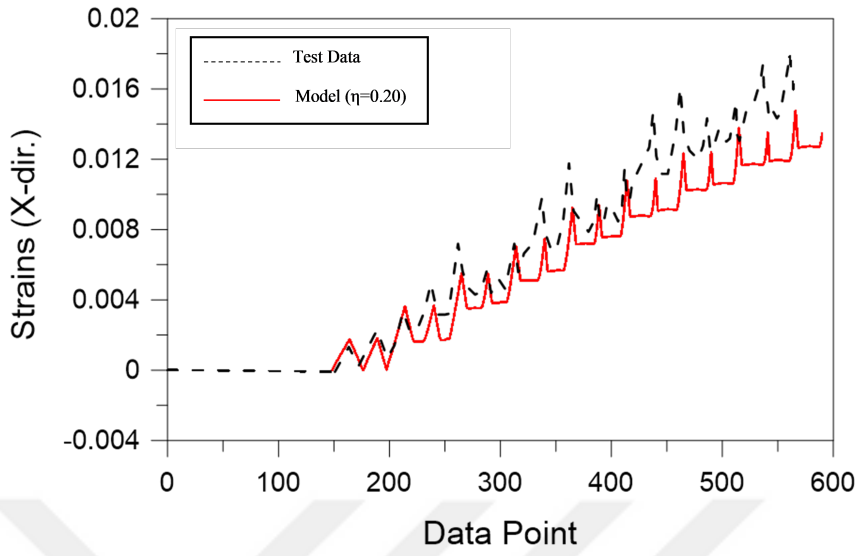

Figure 4.34. CA2: Comparison of Strains in X-direction of Test Data and Model using a friction coefficient of 0.20.

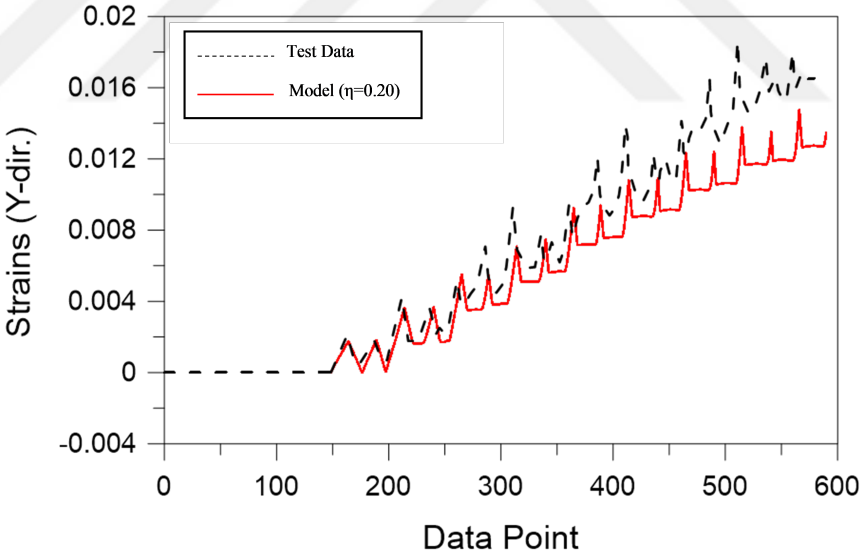

Figure 4.35. CA2: Comparison of Strains in Y-direction of Test Data and Model using a friction coefficient of 0.20.

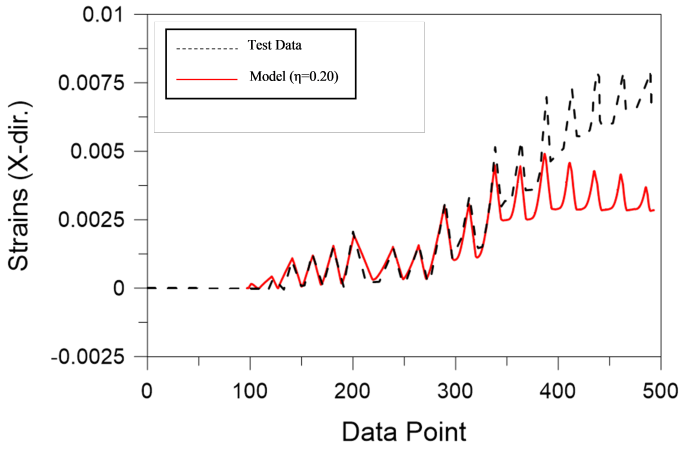

Figure 4.36. CA3: Comparison of Strains in X-direction of Test Data and Model using a friction coefficient of 0.20.

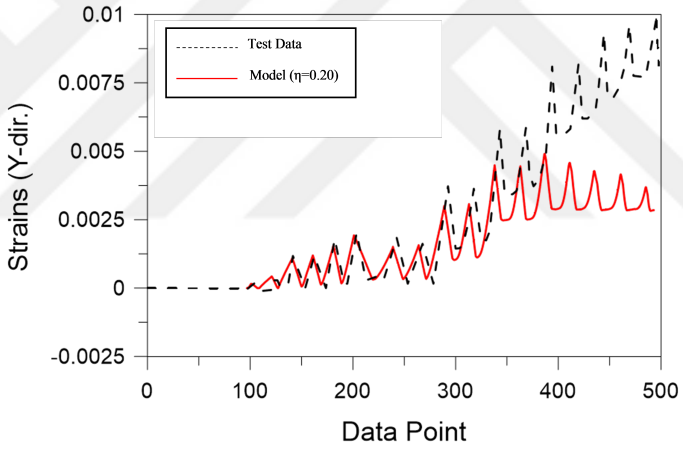

Figure 4.37. CA3: Comparison of Strains in Y-direction of Test Data and Model using a friction coefficient of 0.20.

4.6.9. Local Responses of CB and CD Series Specimens

Specimens CB4 and CD4 incorporated asymmetry either in reinforcement ratios or loading conditions, resulting in asymmetry in the normal strains observed in x and y directions (Figure 4.38 to Figure 4.41). A similar situation is observed for the strain histories predicted by the model. In general, the progression of residual strain, as well as the maximum strain values attained during each cycle or incursions into negative (compressive) values, are well captured.

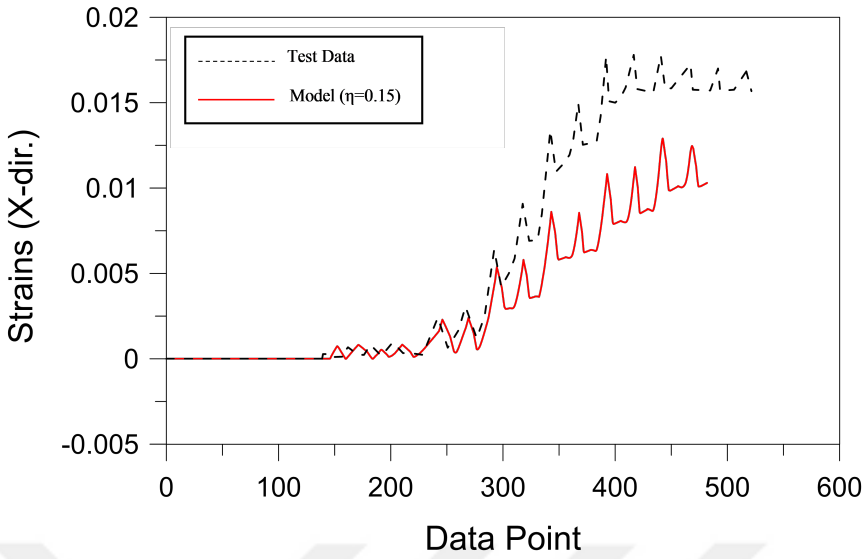

Figure 4.38. CB4: Comparison of Strains in X-direction of Test Data and Model using a friction coefficient of 0.15.

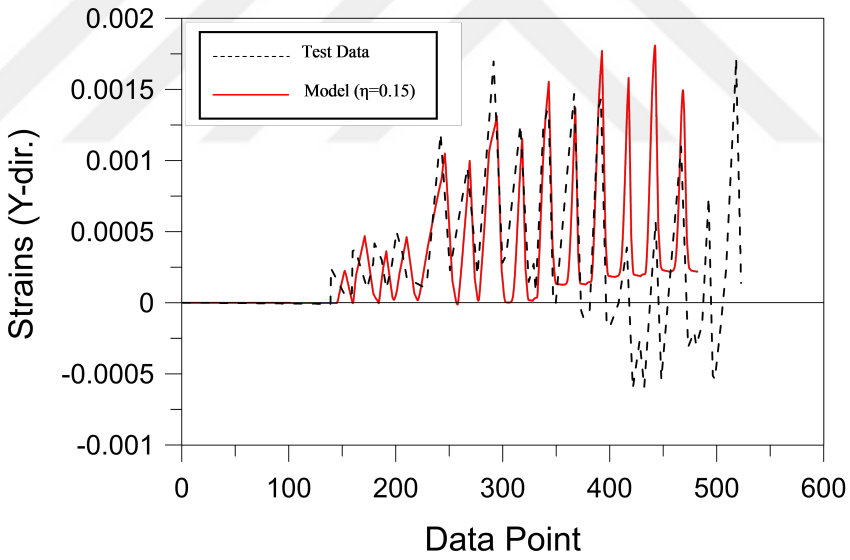

Figure 4.39. CB4: Comparison of Strains in Y-direction of Test Data and Model using a friction coefficient of 0.15.

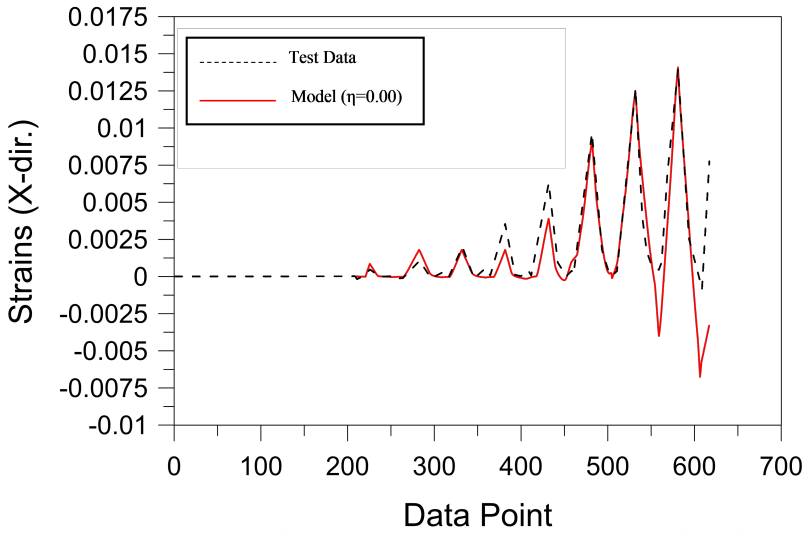

Figure 4.40. CD4: Comparison of Strains in X-direction of Test Data and Model using a friction coefficient of 0.00.

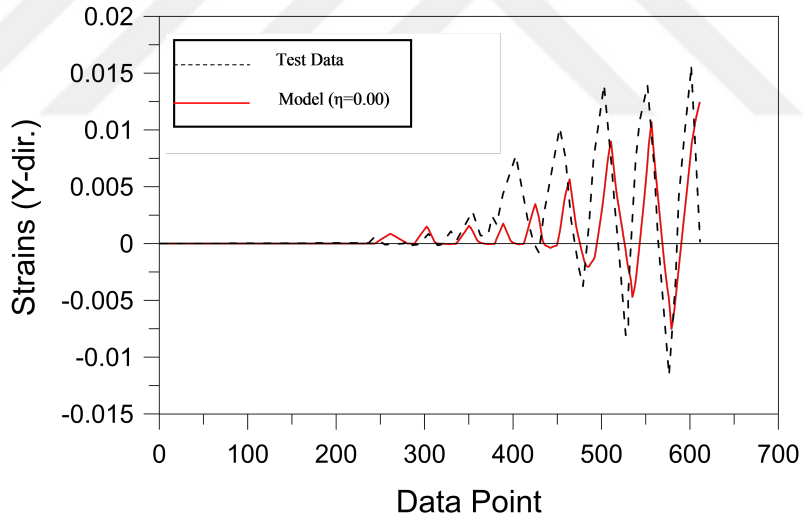

Figure 4.41. CD4: Comparison of Strains in Y-direction of Test Data and Model using a friction coefficient of 0.00.

5. CONCLUSIONS

5.1. Overview

This study focused on improving the formulation of previously-developed reinforced concrete panel model, named as the Fixed-Strut-Angle Model (Ulugtekin, 2010), by incorporating an elasto-plastic shear aggregate interlock constitutive model along crack surfaces, which also considers cyclic degradation in interlock stresses, as well as by implementing an origin-oriented constitutive model for representing dowel action on the reinforcing steel bars, also with consideration of cyclic degradation behavior, in order to better represent the nonlinear hysteretic constitutive (stress vs. strain) behavior of reinforced concrete panel (membrane) elements under plane stress state. Before presenting optimal response predictions of the model, sensitivity analyses were conducted for determination of the coefficient of frictions for specimens that were sensitive to friction across cracks. Following the sensitivity analyses performed on five different panel specimens which were identified to be sensitive to the friction coefficient, ten panel specimens with the identified optimal friction coefficients were modeled and analyzed using Matlab (2012). Global and local response predictions of the model were compared with reinforced concrete panel test results provided by Stevens (1987) and Mansour and Hsu (2005), for experimental validation of improved FSAM. Several conclusions were derived based on the outcomes of this study and their interpretation.

5.2. Conclusions

Based on the analytical results presented in this study, the following conclusions on the characteristics of the FSAM can be reached:

- The improved FSAM has proven to be a relatively simple constitutive model that is capable of simulating the coupled axial/shear stress-strain behavior of reinforced concrete panel elements. Despite its simple formulation and well-defined assumptions, results of the correlation studies conducted in this study indicate

that the FSAM consistently provides reasonably accurate response predictions for RC panels with various reinforcement configurations, subjected to various loading conditions (stress states). The model was shown to generally capture the overall behavioral attributes of most of the RC panel specimens investigated, including the overall shear stress vs. shear strain behavior, cracking shear stress, shear stiffness, cyclic stiffness degradation, ductility, pinching behavior, and failure mode (crushing of concrete vs. yielding of reinforcement).

- Compared to the original FSAM formulation (Ulugtekin, 2010), which neglected the shear transfer mechanisms across cracks, the improved model estimated shear stress capacities and degradation in shear stress vs. strain behavior for most of the panel specimens with improved accuracy, although the friction coefficient for shear stresses along crack surfaces had to be optimized to reach the best correlations between model predictions and test results for each individual specimen.
- Analysing the panel specimens with the improved model indicated that some specimens were sensitive to the friction coefficient value used in the analyses, whereas some of them were not influenced by this parameter. It was observed that specimens with asymmetric reinforcement configuration between x and y directions and inclined reinforcement configurations, as well as the specimens subjected to complicated loading conditions are sensitive to the friction coefficient value selected, since these specimens are prone to more pronounced levels of shear stress transfer across cracks. Based on the analysis results, an optimal range of friction coefficient was identified for each panel test series separately: 0.10 for the SE-series specimens and 0.15-0.20 for most of the C-series specimens.
- Overall, the model was shown to be reliable in simulating the experimentally-measured global (shear stress vs. strain) responses of the panel specimens investigated, as well as predicting the local responses of specimens, although the accuracy of the local response predictions are subject to improvement.
- It was also observed that the improved model did not capture the shear stress capacities and/or degrading behavior in later cycles for certain panel specimens having higher order of asymmetries in their orthogonal reinforcement ratios, meaning the model is less suitable for similar panels (i.e. panels with high order of asymmetrical reinforcements).

5.3. Recommendations for Future Research

Considering the outcomes of this study following research topics are recommended.

- With the improved formulation presented in this study, the FSAM is recommended as a relatively simple yet reliable constitutive model that can be used in finite element model formulations for reinforced concrete walls.
- More refined hysteretic constitutive relationships for representing shear transfer mechanisms across cracks can be implemented in the FSAM formulation for improved accuracy in simulation of both global and local response characteristics of reinforced concrete panels.

REFERENCES

1. Bal, İ., H. Crowley, R. Pinho, and F. Gulay, "Detailed Assessment of Structural Characteristics of Turkish RC Building Stock For Loss Assessment Model", *Soil Dynamics and Earthquake Engineering*, Vol. 28, No.10-11, pp. 914-932, 2018.

2. Belarbi A, T.C. Hsu, "Constitutive Laws of Concrete in Tension and Reinforcing Bars Stiffened By Concrete", *Structural Journal*, Vol. 91, No. 4, pp. 465-474, 1994.

3. Belarbi A, T.C. Hsu, "Constitutive Laws of Softened Concrete in Biaxial Tension Compression", *Structural Journal*, Vol. 92, No. 5, pp. 562-573, 1995.

4. Bentz E.C. "Explaining the Riddle of Tension Stiffening Models for Shear Panel Experiments", *American Society of Civil Engineers Journal of Structural Engineering*, Vol. 131, No. 9, pp. 1422-1425, 2005.

5. Chang G.A., J.B. Mander, *Seismic Energy Based Fatigue Damage Analysis of Bridge Columns: Part I-Evaluation of Seismic Capacity*,NCEER Technical Report No. NCEER-94-0006, National Center for Earthquake Engineering Research, State University of New York at Buffalo, 1994.

6. Clarke, M.J., G.J. Hancock, "A Study of Incremental-Iterative Strategies for Non-Linear Analyses", *International Journal for Numerical Methods in Engineering*, Vol. 29, pp. 1365-1391, 1990.

7. Collins, M.P. and D. Mitchell, *Prestressed Concrete Structures*, Prentice Hall, 1991.

8. Dei Poli S, M. Di Prisco, P.G. Gambarova, "Shear Response Deformations and Subgrade Stiffness of A Dowel Bar Embedded in Concrete", *Structural Journal* , Vol. 89, No. 5, pp. 665-675, 1992.

9. Dulacska H. "Dowel Action of Reinforcement Crossing Cracks in Concrete", *Jour-*

nal Proceedings, Vol. 69, No. 12, pp. 754-757, 1972.

10. Filippou F., E. Popov, V. Bertero, "Effects of Bond Deterioration on Hysteretic Behavior of Reinforced Concrete Joints", *Earthquake Engi- neering Research Center, University of California, Berkeley*, University of California, Berkeley, 1983.

11. Gerin M., P. Adebar, "Simple Rational Model for Reinforced Concrete Subjected to Seismic Shear", *American Society of Civil Engineers Journal of Structural Engineering*, Vol. 135, No. 7, pp. 753-761, 2009.

12. Greek Code for Interventions (KANEPE), *Earthquake Planning and Protection Organization*, Council of Europe European Centre on Preventing and Forecasting of Earthquakes, Athens, 2013.

13. Gullu, M.F., K. Orakcal, *Nonlinear Finite Element Modeling of Reinforced Concrete Structural Walls, Proceedings*, Journal of Earthquake Engineering, 2017.

14. He X, and A. Kwan, "Modeling Dowel Action of Reinforcement Bars for Finite Element Analysis of Concrete Structures", *Computers and Structures*, Vol. 79, No. 6, pp. 595-604, 2001.

15. Hetenyi M.I., *Beams on Elastic Foundation: Theory with Applications in the Elds of Civil and Mechanical Engineering*, University of Michigan, Michigan, 1958.

16. Horoz B., M.F. Gullu, K. Orakcal, "Modeling of Coupled Nonlinear Shear and Flexural Responses in Medium Rise RC walls Proceedings 3rd Conference on Smart Monitoring", *Assessment and Rehabilitation of Civil Structures*, 2015.

17. Hsu, T.C., "Softened Truss Model Theory for Shear and Torsion", *American Concrete Institute Structural Journal*, Vol. 85, No. 6, pp. 624-635, 1988.

18. Hsu, T.C. and L. Zhang, "Tension Stiffening in Reinforced Concrete Membrane Elements", *American Concrete Institute Structural Journal*, Vol. 93, No. 1, pp. 108-115, 1996.

19. Hsu T.C., R.H. Zhu "Softened Membrane Model for Reinforced Concrete Elements in Shear", *American Concrete Institute Structural Journal*, Vol. 99, No. 4, pp. 460-469, 2002.

20. Ince, R., E. Yalcin, and A. Arslan, "Size-Dependent Response of Dowel Action in RC Members", *Engineering Structures*, Vol. 29, pp. 955-961, 2006.

21. Karabulut S., *Nonlinear Response Modelling of Low-Rise Structural Walls*, M.S. Thesis, Bogazici University, 2012.

22. Kolozvari, K.I., *Analytical Modeling of Cyclic Shear - Flexure Interaction in Reinforced Concrete Structural Walls*, Ph.D. Thesis, University of California, Los Angeles, 2013.

23. Mansour M.Y., *Behavior of Reinforced Concrete Elements under Cyclic Shear: Experiments to Theory*, Ph.D. Thesis, Department of Civil Engineering, University of Houston, 2001.

24. Mansour M.Y., T.C. Hsu, J.Y. Lee, "Pinching Effect in Hysteretic Loops of R/C Shear Elements", *Special Publication*, Vol. 205, pp. 293-321, 2002.

25. Mansour M.Y., T.C. Hsu "Behavior of Reinforced Concrete Elements under Cyclic Shear. I: Experiments", *Journal of Structural Engineering*, Vol. 131, No. 1, pp. 44-53, 2005.

26. Mansour M.Y., T.C. Hsu, "Behavior of Reinforced Concrete Elements under Cyclic Shear. II: Theoretical Model", *Journal of Structural Engineering*, Vol. 131, No. 1, pp. 54-65, 2005.

27. Matlab M., *The Language of Technical Computing*, The Math Works, Inc., Massachusetts USA, 2012.

28. Mau, S.T. and T.C. Hsu, "Shear Design and Analysis of Low-Rise Structural Walls", *American Concrete Institute Structural Journal*, Vol. 83, No. 2, pp. 306-

315, 1986.

29. Mau, S.T. and T.C. Hsu, "Shear Behavior of Reinforced Concrete Framed Wall Panels With Vertical Loads", *American Concrete Institute Structural Journal*, Vol. 84, No. 3, pp. 228-234, 1987.

30. McKenna F., G.L. Fenves, M.H. Scott and B. Jeremic, *Open System for Earthquake Engineering Simulation (OpenSees)*, Pacific Earthquake Engineering Research Center, University of California, Berkeley, CA 2000.

31. Menegotto M, E. Pinto, *Method of Analysis for Cyclically Loaded Reinforced Concrete Plane Frames Including Changes in Geometry and Non-Elastic Behavior of Elements Under Combined Normal Force and Bending. Proceedings*, Proceedings, IABSE Symposium on Resistance and Ultimate Deformability of Structures Acted on by Well-Defined Repeated Loads, Lisbon, Portugal, 1973.

32. Mitchell, D., M.P. Collins, "Diagonal Compression Field Theory A Rational Model for Structural Concrete in Pure Torsion", *American Concrete Institute Structural Journal*, Vol. 71, No. 8, pp. 396-408, 1974.

33. Oesterle, R.G., A.E. Fiorato, L.S. Johal, J.E. Carpenter, H.G. Russell, and W.G. Corley, *Earthquake resistant structural walls-Tests of isolated walls*, Report to National Science Foundation, Grant No. GI-43880, Research and Development Construction Technology Laboratories Portland Cement Association, Skokie, Illinois, 1976.

34. Ohmori, N., T. Takahashi, N. Inoue, K. Kurihara, S. Watanabe, "Experimental Studies on Nonlinear Behaviors of Reinforced Concrete Panels Subjected to Cyclic in-plane Shear", *Proceedings of Architectural Institute of Japan*, Vol. 403, pp. 105-117, 1989.

35. Okamoto, S., S. Shiomi and K. Yamabe, "Earthquake Resistance of Prestressed Concrete Structures", *Architectural Institute of Japan Proceedings*, pp. 1251-1252,

1976.

36. Orakcal K., D. Ulugtekin, L.M. Massone, "Constitutive Modeling of Reinforced Concrete Panel Behavior Under Cyclic Loading, Proceedings", *Proceedings, 15th World Conference on Earthquake Engineering*, Lisbon, Portugal, No. 3573, 2012.

37. Palermo D., F.J. Vecchio, "Compression Field Modeling of Reinforced Concrete Subjected to Reversed Loading: Formulation", *American Concrete Institute Structural Journal*, Vol. 100, No. 5, pp. 616-625, 2003.

38. Palieraki V, E. Vintzileou, C. Zeris, "Behaviour of Interfaces in Repaired / Strengthened RC Elements Subjected to Cyclic Actions: Experiments And Modelling", *Proceedings, 3rd international symposium on life-cycle and sustainability of civil infrastructure systems (IALCCE'12)*, Vienna, Austria; 2012.

39. Pang X.D., T.C. Hsu, "Behavior of Reinforced Concrete Membrane Elements in Shear", *Structural Journal*, Vol. 92, No. 6, pp. 665-679, 1995.

40. Pang D., T.C. Hsu, "Fixed Angle Softened Truss Model for Reinforced Concrete", *American Concrete Institute Structural Journal*, Vol. 93, No. 2, pp. 197-207, 1996.

41. Popovics, S., "A Numerical Approach to the Complete Stress-Strain Curve of Concrete", *Cement and Concrete Research*, Vol. 3, No. 4, pp. 583-599, 1973.

42. Powell, G. and J. Simons, "Improved Iteration Strategy for Nonlinear Structures", *International Journal for Numerical Methods in Engineering*, Vol.17, pp. 1455-1467, 1981.

43. Tassios, T.P. and E.N. Vintzileou, "Mathematical Models for Dowel Action under Monotonic Conditions", *Magazine of Concrete Research*, Vol. 38, No. 134, pp. 13-22, 1986.

44. Tassios, T.P., E.N. Vintzeleou, "Concrete-to-Concrete Friction", *Journal of Structural Engineering*, Vol. 113, No. 4, pp. 832-849, 1987.

45. Sinha B.P., K.H. Gerstle and L.G. Tulin, "Stress-Strain Relations for Concrete under Cyclic Loading", *Journal of the American Concrete Institute*, Vol. 61, No. 2, pp. 195-211, 1964.

46. Karsan, I.D. and J.O. Jirsa, "Behavior of Concrete under Compressive Loadings", *American Society of Civil Engineers Journal of the Structural Division*, Vol. 95, No. ST12, pp. 2543-2563, 1969.

47. Spooner, D.C. and J.W. Dougill, "A Quantitative Assessment of Damage Sustained in Concrete During Compression Loading", *Magazine of Concrete Research*, Vol. 27, No. 92, pp. 151-160, 1975.

48. Stevens N.J., *Analytical Modeling of Reinforced Concrete Subjected to Monotonic and Reversed Loadings*, Ph.D. Thesis, Department of Civil Engineering, University of Toronto, 1987.

49. Stevens N.J., M. Uzumeri, M.P. Collins, "Reinforced Concrete Subjected to Eversed Cyclic Shear Experiments and Constitutive Model", *American Concrete Institute Structural Journal*, Vol. 88, No. 2, pp. 135-146, 1991.

50. Soroushian P., K. Obaseki, M.C. Rojas, "Bearing Strength and Stiffness of Concrete under Reinforcing Bars", *Materials Journal*, Vol. 84, No. 3, pp. 179-184, 1987.

51. Tanigawa, Y. and Y. Uchida, "Hysteretic Characteristics of Concrete in the Domain of High Compressive Strain", *Proceedings of Annual Architectural Institute of Japan (AIJ) Convention, Japan*, pp. 449-450, 1979.

52. Tsai W.T., "Uniaxial Compressional Stress-Strain Relation of Concrete", *Journal of Structural Engineering*, Vol. 114, No. 9, pp. 2133-2136, 1988.

53. Thermou, G.E., V.K. Papanikolaou, A.J. Kappos, "Flexural Behavior of Reinforced Concrete Jacketed Columns under Reversed Cyclic Loading", *Engineering*

Structures, Vol. 76, pp. 270-282, 2014.

54. Tassios, T.S., "Fundamental Mechanisms of Force-Transfer across Reinforced Concrete Critical Interfaces", *Workshop on Cultural Education in Germany and Turkey*, pp. 381-397, 1986.

55. Ulugtekin D., *Analytical Modeling of Reinforced Concrete Panel Elements under Reversed Cyclic Loadings*, M.S. Thesis, Bogazici University, Istanbul, Turkey, 2010.

56. Vassilopoulou I, P. Tassios, "Shear Transfer Capacity along a RC Crack under Cyclic Sliding. In: Proceedings Fib Symposium", *Proceedings, FIB Symposium*, pp. 271, 2003.

57. Vecchio, F.J. and M.P. Collins, "The Modified Compression-Field Theory for Reinforced Concrete Elements Subjected to Shear", *American Concrete Institute Structural Journal*, Vol. 83, No. 2, pp. 219-231, 1986.

58. Vecchio F.J., M.P. Collins, "Compression Response of Cracked Reinforced Concrete", *American Society of Civil Engineers Journal of Structural Engineering*, Vol. 119, No. 12, pp. 3590-3610, 1993.

59. Vecchio, F.J., "Towards Cyclic Load Modeling of Reinforced Concrete", *American Concrete Institute Structural Journal*, Vol. 96, No. 2, pp. 193-202, 1999.

60. Vecchio, F.J., "Disturbed Stress Field Model for Reinforced Concrete: Formulation", *American Society of Civil Engineers Journal of Structural Engineering*, Vol. 126, No. 9, pp. 1070-1077, 2000.